

# Supersymmetry and the LHC Inverse Problem

Nima Arkani-Hamed<sup>1</sup>, Gordon L. Kane<sup>2</sup>, Jesse Thaler<sup>1</sup>, and Lian-Tao Wang<sup>1</sup>

<sup>1</sup> *Jefferson Laboratory of Physics, Harvard University,  
Cambridge, Massachusetts 02138, USA*

<sup>2</sup> *Physics Department, University of Michigan and MCTP  
Ann Arbor, Michigan 48109, USA*

## Abstract

Given experimental evidence at the LHC for physics beyond the standard model, how can we determine the nature of the underlying theory? We initiate an approach to studying the “inverse map” from the space of LHC signatures to the parameter space of theoretical models within the context of low-energy supersymmetry, using 1808 LHC observables including essentially all those suggested in the literature and a 15 dimensional parametrization of the supersymmetric standard model. We show that the inverse map of a point in signature space consists of a number of isolated islands in parameter space, indicating the existence of “degeneracies”—qualitatively different models with the same LHC signatures. The degeneracies have simple physical characterizations, largely reflecting discrete ambiguities in electroweak-ino spectrum, accompanied by small adjustments for the remaining soft parameters. The number of degeneracies falls in the range  $1 < d < 100$ , depending on whether or not sleptons are copiously produced in cascade decays. This number is large enough to represent a clear challenge but small enough to encourage looking for new observables that can further break the degeneracies and determine at the LHC most of the SUSY physics we care about. Degeneracies occur because signatures are not independent, and our approach allows testing of any new signature for its independence. Our methods can also be applied to any other theory of physics beyond the standard model, allowing one to study how model footprints differ in signature space and to test ways of distinguishing qualitatively different possibilities for new physics at the LHC.

# 1 The LHC Inverse Problem

With the imminent start of the LHC in 2007, particle physics is on the threshold of its most exciting period in over thirty years. The secrets of the TeV scale will begin to be revealed, and whatever is found is likely to have profound implications for fundamental physics. With only two years to go, what are the most pressing remaining open questions in physics beyond the standard model? Over the last two decades, many models of weak scale physics have been proposed, starting with the early proposals of supersymmetry [1] and technicolor [2], through to the more recent ideas of large and warped dimensions [3, 4], and the little Higgs [5]. The last three years have seen an explosion of differing models—ranging from Higgsless models [6], composite Higgs in warped compactifications [7] and other warped models [8, 9], twin Higgs [10], and SUSY little Higgs models [11]—largely arising from combining previous ideas in a variety of ways. More recently, orthogonal “un-natural” directions have also been opened up, inspired by the possibility of an enormous landscape of vacua in string theory, beginning with the proposal of split supersymmetry [12] and other minimal models for dark matter and unification [13, 14].

However, it is clear that the era of speculation and model-building is near an end—we will very soon get a direct hint for what is going on from early LHC data. It is unlikely that exploring the  $(N + 2)$ nd variation on the  $(N + 1)$ st mechanism for electroweak symmetry breaking is particularly important at this moment in time. Unless some qualitatively new ideas and associated signals are involved, one might as well wait and see what nature tells us before investing a lot of time on detailed model variations.

Instead, there is another problem, far more urgent especially as the LHC draws near, that has received less attention than model-building. How will we determine the underlying new physics from LHC data? Of course the first important question is: how will we know there is *any* new physics beyond the standard model? It is possible that the signals will be sufficiently spectacular as to immediately tell us there is new physics and narrow the space of possibilities to a very small number. For instance, if the LHC finds evidence for a colored particle decaying an observable distance from the beamline, this would look a lot like split SUSY or perhaps other models with nearly stable colored particles, but not anything like a garden-variety supersymmetric model.

Even without such dramatic signatures, if there are new colored particles beneath the  $\sim 2$  TeV scale that are produced and decay to SM particles, we can fairly quickly be convinced of the existence of new physics. But determining the properties of the underlying model becomes more challenging, even at a rough level. For instance, can we know if we

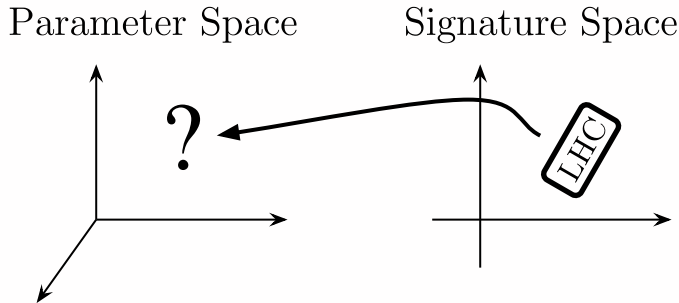


Figure 1: The Inverse Map from LHC Observables to Theoretical Models. Given observed signals for physics beyond the standard model, how can we determine the underlying theoretical model?

have discovered SUSY, or are the signals with trileptons and missing energy due to extra dimensions with KK parity [15], or little Higgs theories with  $T$ -parity [16]? Despite some recent studies [17, 18, 19, 20, 21, 22, 23, 24], not much systematic work has been done on this “inverse” problem [25, 26]. Let’s suppose even that we are working in the context of low-energy SUSY with minimal field content. Will we be able to determine even qualitative properties of the spectrum? Can we, for instance, tell even roughly whether or not the gaugino masses are consistent with GUT scale unification? Whether the LSP is a good candidate for Dark Matter?

Instead of addressing this question, most of the work on collider phenomenology to date has been done in the “forward” direction, studying the map from parameter or model space into the space of observable collider signatures. The signals for a specific model are studied in great detail, with the goal of seeing how well the parameters of the model can be measured or constrained. Often, many of the signals are tailor-made to the model at hand and aren’t effective for other models, particularly not for the general case. To make the studies tractable, they are usually performed within simplified models with very few parameters—in the context of SUSY, for instance, these have been carried out with mSUGRA, gauge mediated and anomaly mediated SUSY breaking [27, 28, 29, 30, 31, 32, 33], for several recent studies, see [34, 35, 36, 37, 38, 39, 40]. Presumably, the hope is that if enough models are simulated in the forward direction, we will gain familiarity with the associated signals and will be able to spot them if they arise at the LHC.

But the LHC inverse problem—studying the map from LHC signatures to weak scale models as in figure 1—is more interesting, important and challenging. At a hadron collider, it is difficult to directly measure masses and other properties of new particles, a problem exacerbated in SUSY by the escaping LSPs carrying away missing energy. Plus, any signal

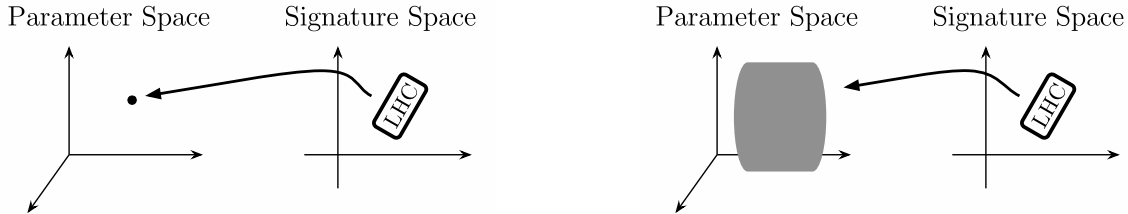


Figure 2: The Inverse Map in the Best and Worst of All Possible Worlds. Ideally, the image of LHC data onto parameter space would specify an unique underlying model. In the most pessimistic scenario, LHC data would suggest the physics beyond the standard model without giving us any clues as which model describes the new physics.

is likely to receive contributions from multiple channels, and the signals that are reliably observable are more limited. A given set of observations at the LHC select a small region point in signature space, whose size is determined by both by intrinsic statistical/quantum ( $\sqrt{N}$ ) fluctuations as well as by experimental errors. The question is, what does the inverse map back to parameter space look like? Even very basic issues are open—for instance, is this map one-to-one?

As shown in figure 2, in the best of all possible worlds, the inverse map from a small region in signature space would pick out a small region in parameter space, so that the underlying model would be uniquely picked out, and better measurements of the signals would yield a more accurate determination of the model parameters. In the worst of all possible worlds, the inverse map into parameter space would fill out a huge continuously connected region of parameter space, giving us no handle on even the basic structure of the underlying theory.

In this paper, we initiate a systematic approach to the LHC inverse problem in the context of low-energy SUSY. As we will see, in SUSY the actual picture is an intermediate one—the inverse map consists of a number of isolated islands in parameter space as in figure 3. While each island is small, there are a number of them corresponding to qualitatively different models. For obvious reasons we call these “degeneracies”—different models with the same LHC signatures. We will be able to give a simple physical interpretations of the main kinds of degeneracies, which arise largely from discrete ambiguities in the electroweak-ino sector.

In the next section, we describe our approach to understanding the map from signature space to parameter space, and describe the simple statistical techniques that allow us to indirectly infer the expected number of models with degenerate LHC signals. In section 3, we then summarize our picture of the inverse map, together with an outline of a simple physical characterization of the dominant source of degeneracies. In section 4, we present the details of our specific study, including the MSSM parameter space we scanned and the 1808

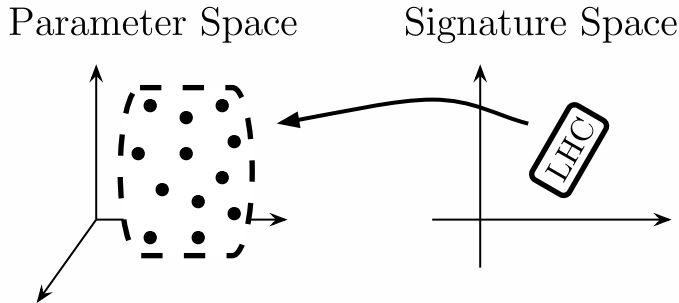


Figure 3: Our Picture of the Inverse Map. In the context of low-energy supersymmetry, we find that the inverse map of LHC data consists of a number of disconnected and widely separated regions in parameter space. This indicates the presence of degeneracies—different underlying models that share the same LHC signatures.

LHC signals we considered. In sections 5 and 6, we give a more detailed characterization of degeneracies and provide specific examples of pairs of degenerate models exemplifying each class of degeneracies. Part of the reason for the degeneracies is that, in most of our parameter scan, on-shell sleptons are not copiously produced in cascade decay chains, so there is less leptonic information. In section 7, we do a dedicated scan over a parameter space where sleptons are typically present in the decay chains, and find that as expected, the number of degeneracies is significantly smaller. In sections 8 and 9, we describe possible improvements and extensions to our work and outline how one should use our study after a real discovery at the LHC. We end with a discussion and outlook on future work in this area.

## 2 From Parameters to Signatures and Back

### 2.1 Parameter and Signature Space

Before studying the inverse map from signature space to parameter space, we should specify what each of these spaces are. Of course, the most pressing question at the LHC will be to figure out whether there is *any* evidence for physics beyond the standard model, and then most broadly what theoretical framework best describes the new physics—for instance is it SUSY, or strong dynamics, or something else? As has been increasingly appreciated over the last couple of years, even here there are possibilities for degeneracies. In particular, any model with a stable particle protected by a parity symmetry has similar looking missing energy signals as SUSY, and it is a challenge to decisively distinguish the models. As far as we can see, there is no systematic approach to this problem yet.

But there is also an analog of the inverse problem purely within the context of low-energy SUSY. The parameter space of the model is so huge, and gives rise to such a large range of possible signals, that we can already ask, even assuming we have low-energy SUSY, whether we can even roughly determine the correct region of parameter space from LHC data. In this context, the “parameter space” is clear—fixing for instance the minimal field content of the supersymmetric standard model, we can vary the  $\sim 105$  soft parameters of the theory. In practice, this is much too large a number, and it is useful to consider a smaller subset that still captures much of the variety of physics to be expected. Many of the 105 soft parameters are relevant only to flavor physics and do not have much effect on collider physics. These consist of three gaugino masses  $M_{1,2,3}$ , the Higgsino mass parameter  $\mu$ , degenerate soft masses for the first two generations of  $Q, U^c, D^c, L, E^c$  fields (in order to avoid large flavor violations), and separate soft terms for the third generation scalars. If we also include  $\tan\beta$ , the ratio of the up- and down-type Higgs vevs, this gives a total of 15 parameters.

The “signature space” is also easily defined, as we will do in more detail in section 4.1. After imposing the appropriate cuts, we associate a number with every LHC observable. For instance, any number count of events of a particular kind is a direction in signature space. Any kinematic histogram can be divided up into deciles, and the boundaries of each decile is a direction in signature space. In this way, we quickly get a huge dimensionality for signature space—the LHC observables in our study span 1808 dimensions.

Since signature space has a much higher dimensionality than parameter space, naively one would think that the inverse map from signature to parameter space would be unique. Actually, this is incorrect, largely because the signatures tend to be highly correlated with each other, so the effective dimensionality of signature space is much smaller. In fact, we can imagine dividing signature space up into bins, with size determined by statistical fluctuations and experimental errors. Even scanning over all possible MSSM parameters, the number of bins in signature space—the number of experimentally distinguishable outcomes at the LHC—is not enormously large. One of our results will be a quantitative measure of this number which will help us understand important aspects of the inverse map.

An obvious strategy for studying the inverse map is to simply simulate the MSSM in all regions of its parameter space. For instance, we can imagine taking each soft mass parameter in 100 GeV increments between, say, 100 GeV and 1 TeV. Even fixing  $\tan\beta$  and taking our simplified 14 relevant soft parameters at the LHC, this is a total of  $\sim 10^{14}$  models. In practice it is impossible to simulate so many models—simulating the first year of LHC data for a single SUSY model with fast detector simulation takes about 1 CPU hour. This is why so many studies are performed in models with a much smaller dimension parameter space,

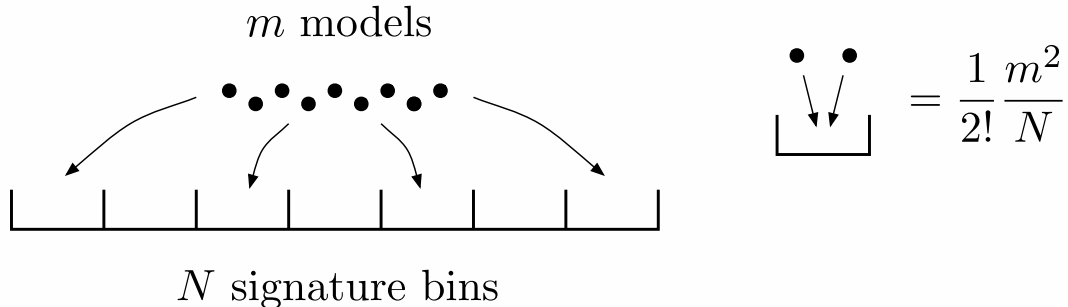


Figure 4: The Birthday Problem for the MSSM. We simulate  $m$  models and associate each model with a bin in signature space. For  $m \ll N$  it is unlikely for any given pair of models to share the same LHC signatures, but there is a statistical expectation value  $N_2 \sim m^2/(2N)$  for the total number of pairs that end up in the same bin.

like the 5 dimensional parameter space of mSUGRA.

## 2.2 Statistics and the Birthday Problem

However, we can get a good idea of what the inverse map looks like even with a large parameter space without having to simulate so many models. We do this by simulating  $m$  models, but then comparing the signatures between all  $m(m - 1)/2$  pairs of models. This gives us statistical leverage and also allows us to determine gross properties of signature space, including its real effective dimensionality as well as the the total number of “bins” or experimentally distinguishable models.

We can do all of this because of the famous “birthday problem” shown in figure 4. To take a simple analogy—suppose we throw balls into a box with  $N$  bins; we can’t see inside the box so we don’t know how big  $N$  is. But the balls are sticky, so that if two balls land in the same bin, they stick together. We can throw in as many balls as we want, and then empty the box. One might think that to determine  $N$ , one has to throw in  $m = N$  balls to cover all possible bins, and then the pigeonhole principle would guarantee seeing a pair of balls stuck together when  $m = N + 1$ , but this is not the case. If we assume that the balls fall into the bins randomly, on average the number of bins with  $p$  balls  $N_p$  is<sup>1</sup>

$$N_p \sim \frac{m^p}{p! N^{p-1}}. \tag{1}$$

In particular, the number of doubles is  $N_2 = m^2/(2N)$ . So, when the balls are dumped

---

<sup>1</sup>This definition of  $N_p$  is still approximately true even for large  $m$  and small  $N$  if we say that a bin with  $q$  balls makes a contribution of  $q$  choose  $p$  to the expectation value of  $N_p$ .

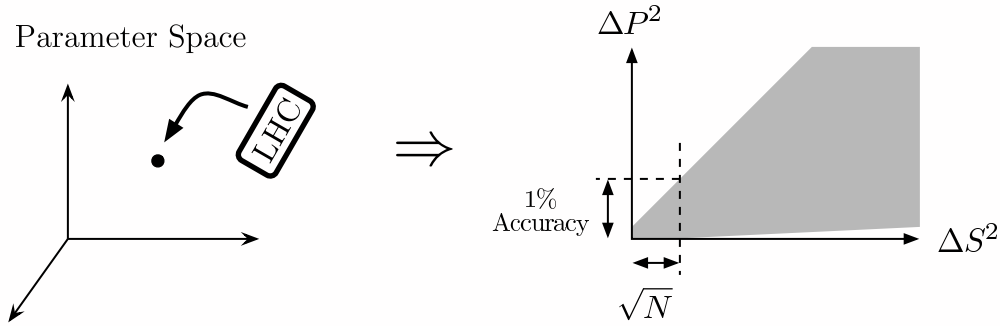


Figure 5: The  $(\Delta S^2, \Delta P^2)$  plot in the best of all possible worlds. The expected confidence range on model parameters is defined by the maximum value of  $\Delta P^2$  at the  $\Delta S^2$  corresponding to statistical fluctuations.

out of the box, we can see how many doubles  $N_2$  there are, and this allows us to determine  $N$  as  $N = m^2/(2N_2)$ . Furthermore, if we saw some triples and quadruples too, we could test our hypothesis by seeing whether the value of  $N$  we extract from all of them are consistent with each other. Clearly, for this pair-wise counting strategy to be effective, we have to have  $m \sim \sqrt{N}$  to have at least a few doubles, but this is a big improvement over the naive expectation that we need  $m \sim N$ .

We follow this strategy in our study. We simulate  $m$  models and associate each with a point in LHC signature space. Any *pair* of models has an associated distance  $\Delta P^2$  in parameter space and  $\Delta S^2$  in signature space<sup>2</sup>. We can look at a 2D plot of the points  $(\Delta S^2, \Delta P^2)$  for all  $m(m-1)/2$  pairs of models. In the best possible situation, this plot would look like a narrow triangle, as in figure 5. The minimal  $\Delta S^2$  corresponding to  $\sqrt{N}$  error would correspond to a small  $\Delta P^2$  in parameter space and larger  $\Delta S^2$  would be associated with larger  $\Delta P^2$ .

### 2.3 Degeneracies

The real situation with the MSSM is rather different—the plot for the models we simulate is shown in figures 6 and 7. We will specify our parameters and signatures in more detail in section 4. For the present it suffices to say that  $m = 43026$  MSSMs were simulated. The vertical dashed line in figure 7 marks  $\Delta S^2 = 0.285$ , corresponding to the distance in signature space when the *same model* is repeatedly simulated, giving us a measure of the size of statistical fluctuations.

<sup>2</sup>See section 4.3 for precise definitions of  $\Delta P^2$  and  $\Delta S^2$ .

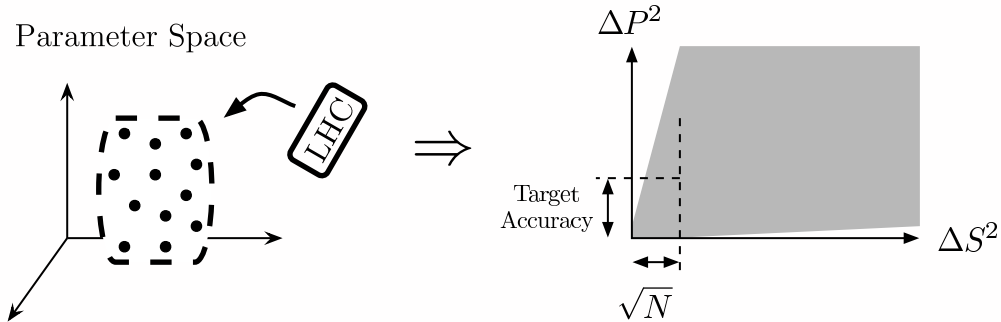


Figure 6: A cartoon of  $(\Delta S^2, \Delta P^2)$  plot in the general MSSM. At the  $\Delta S^2$  value corresponding to statistical fluctuations, the maximum value of  $\Delta P^2$  exceeds the target accuracy on model parameters. While it is possible to change the target accuracy value to formally decrease the number of degeneracies, for any reasonable choice (such as 10% or 20% error), there is still a sizable number of degenerate pairs. Notice that target accuracies of the parameters usually correspond to a much larger region in the parameter space than that is occupied any small island. This corresponds to the existence of many “cliffs”, see section 2.4.

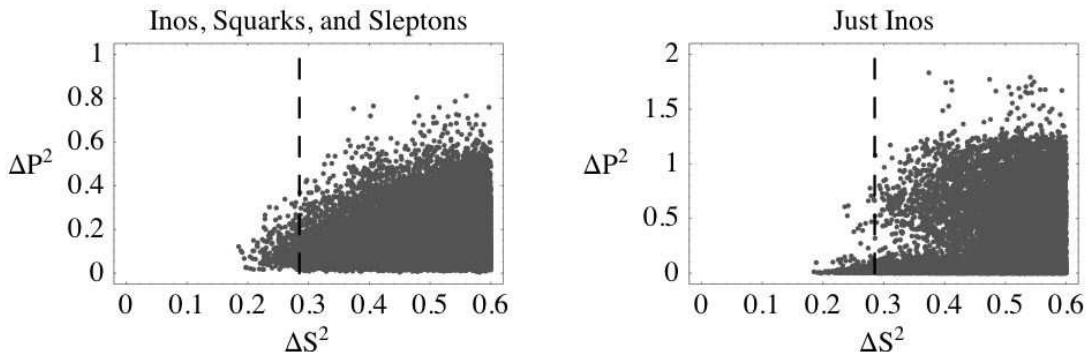


Figure 7: The  $(\Delta S^2, \Delta P^2)$  plot for the MSSM. In the left plot, we measure  $\Delta P^2$  using the 14 mass parameter we scan, where  $\Delta P^2 \sim 0.01$  roughly corresponds to 10% accuracy in all parameters. The position of the vertical dashed line corresponds to the distance in signature space from statistical fluctuations, so the fact that there is a sizable number of model pairs to the left of this line with large  $\Delta P^2$  indicates the presence of degeneracies. The right plot shows the same models with  $\Delta P^2$  measured only using the gaugino and higgsino mass parameters. As we will explain in section 3, the break in the plot between small and large  $\Delta P^2$  comes from a bimodal behavior in the electroweak-ino sector, which explains the dominant reason why there are degeneracies in the MSSM. Note that only a small number of pairs are shown on these plots; the  $\Delta S^2$  values extend out to  $\Delta S^2 \gtrsim 600$ .

The most striking feature of this plot is the clear presence of a relatively large number of degenerate models—there are many points with small  $\Delta S^2$  but large  $\Delta P^2$ . (As we explain in section 4.3,  $\Delta P^2 \sim 0.01$  corresponds to parameters matching to 10% accuracy.) The 43026 models represent a very sparse sampling of the 14 dimensional parameter space, and yet 283 pairs of models share indistinguishable signatures!

From our “birthday problem” picture, this is clear evidence that the number of effective “bins” in signature space is not enormously large. The expected number of signature bins is

$$N_{\text{sig}} \sim \frac{m^2}{2N_2} \sim 3.3 \times 10^6. \quad (2)$$

As described in appendix A, we can confirm that this picture is correct by extracting a value of  $N$  also by looking at the number of triplets and quadruplets of models with the same signatures. The value of  $N$  extracted in this way is indeed of the same order of magnitude as above. The fit can be further improved by taking into account that some fraction of the bins are more likely to be populated than others.

Our estimate for  $N_{\text{sig}}$  gives us a good idea of the number of distinguishable bins in signature space—that is, the number of *possible distinguishable* MSSMs in the parameter space we scanned. But the actual number of degeneracies we care about is criterion dependent. For instance, if two models are degenerate with mass parameters differing by, say, only 5% from one another, then we may not wish to count these models as being “really different”. We can define what we mean by “good pairs” which are sufficiently close in parameter space that we would expect them to be close in signature space. Given such a criterion, the expectation value for the number of degeneracies from figure 8 is

$$\langle \text{degeneracies} \rangle = \frac{\text{number of pairs close in signature space}}{\text{number of “good” pairs}}. \quad (3)$$

For instance, for our set of 283 LHC indistinguishable pairs, we can decide to declare two models “the same” if they have the same ordering of the ino spectrum. In this case, the number of degeneracies is  $\langle d \rangle = 4.4$ —that is, for a given model, there are about 4 other models with the same LHC signatures but a *different* ino ordering. Or we can decide that two models with ino masses within 10 percent of each other are “the same”. In this case,  $\langle d \rangle = 12.9$ , so we expect for any given model, there are about 12 others with the same LHC signatures but with ino masses differing by more than 10 percent. There are only 2 out of the 283 pairs whose ino and squark masses match to 10%, so using that criteria we would expect  $\langle d \rangle \sim 140$ . In figure 9, we show how the number of degeneracies changes as we adjust the fractional acceptance in parameter space between pairs of models, showing that the source

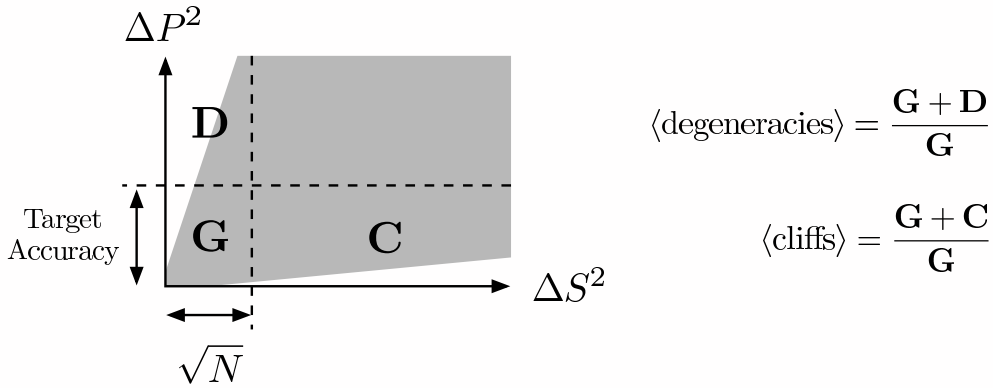


Figure 8: A cartoon showing how to count the expectation value for the number of degeneracies and cliffs. Region **G** corresponds to “good pairs” of models that are close both in parameter space and signature space. Region **D** correspond to pairs of models that are degenerate, *i.e.* close in signature space but well separated in parameter space. Region **C** corresponds to “cliffs”, where the distance between models in signature space is large despite the models’ proximity in parameter space.

of degeneracies is not coming only from large error bars on individual parameters but also from discrete choices in the SUSY spectrum.

So we see that the number of degeneracies is  $\mathcal{O}(10 - 100)$  with the criteria we have specified. We can get a rough idea of whether this number is in the right ballpark by estimating the number of degeneracies in a different way. We have determined that there are  $N_{\text{sig}} \sim 3 \times 10^6$  possibly distinguishable MSSMs. We can also estimate the number of “different” models  $N_{\text{models}}$  we have in our parameter space based on the parameter ranges given in section 4.2. Assuming that LHC signatures are sensitive to gluino mass variations of 50 GeV, squark mass variations of 75 GeV, and electroweak-ino mass variations of 100 GeV, then<sup>3</sup>

$$N_{\text{models}} \sim 8 \times 5^6 \times 9^3 \sim 10^8. \quad (4)$$

Since  $N_{\text{models}} > N_{\text{sig}}$ , by the pigeonhole principle there *must* be degeneracies. Furthermore, a rough estimate for the number should be

$$\langle \text{degeneracies} \rangle \sim \frac{N_{\text{models}}}{N_{\text{sig}}} \sim 30 \quad (5)$$

which is indeed consistent with our first estimate using equation (3).

---

<sup>3</sup>These values are chosen by estimating the local variation in mass parameters from the  $(\Delta S^2, \Delta P^2)$  plots in section 5.

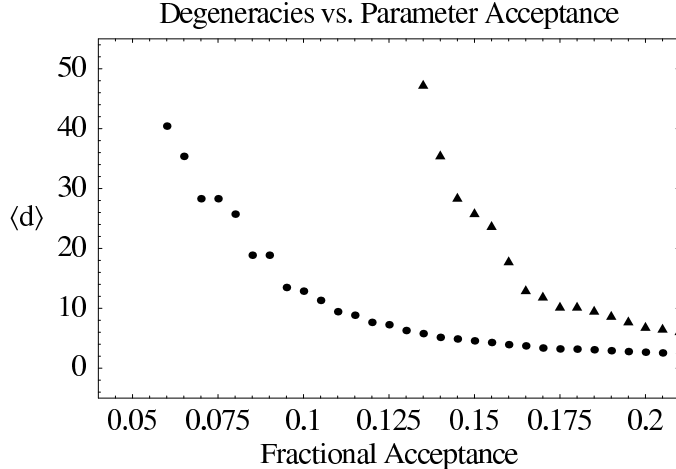


Figure 9: Number of degeneracies as a function of allowed fractional error. Triangles correspond to imposing fractional acceptance on gaugino, higgsino, and squark parameters. Dots correspond to just imposing fractional acceptance on the inos. The fact that the number of degeneracies asymptotes to 2 indicates that the degeneracies are not caused simply by the presence of large error bars on model parameters but also because of discrete choices in the spectrum.

## 2.4 Cliffs

Another important feature of the  $(\Delta S^2, \Delta P^2)$  plot is the population of points along the horizontal axis, which shows that there are models with small distance in parameter space but large differences in signature space. These indicate the existence of “cliffs” in model space—small parameter changes can give rise to large changes in the signatures. In particular, this suggests that in any local region of parameter space, the map to LHC signature is essentially one-to-one.

We can easily quantify this notion. Given any criterion for whether two models share the same “parameter bin”, we can find the total number of pairs of models which are close in parameter space and compare with the number which are close in both signature space and parameter space. This defines an expected value of cliffs, *i.e.* the chance that two models within the same parameter bin end up in the same signature bin.

$$\langle \text{cliffs} \rangle = \frac{\text{number of pairs close in parameter space}}{\text{number of “good” pairs}}. \quad (6)$$

We can look at a plot of the number of cliffs as a function of changing the signature cut that defines “good” pairs. Depending on the criteria for closeness in parameter space, we see that the number of cliffs is  $\mathcal{O}(10^3)$ – $\mathcal{O}(10^4)$ , showing that a single bin in parameter space maps to many different bins in signature space. This confirms the picture in figure 3 that the isolated

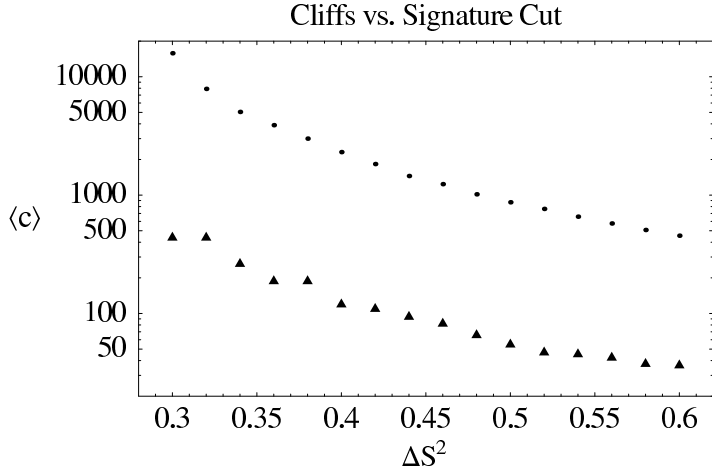


Figure 10: Number of cliffs as a function of signature cut.  $(\Delta S)^2 = 0.285$  corresponds to statistical fluctuations. Triangles correspond to imposing 10% percent acceptance on gaugino, higgsino, and squark parameters. Dots correspond to imposing 10% percent acceptance on just the inos. The large number of cliffs indicate the strong sensitivity of LHC observables in local regions of parameter space.

regions in parameter space that map to the same signature bin are indeed “small”.

## 2.5 Effective Dimensionality of Signature Space

Formally, our signature space is very high dimensional. Of course, we are mapping a 15 dimensional parameter space onto signature space, so we do not expect the signature space manifold spanned by SUSY models to be more than 15 dimensional. However, the existence of degeneracies strongly suggests that there are huge correlations between the signatures, such that the actual dimensionality of the space populated by SUSY models is far smaller.

We can quantify this simply by looking at how the number of degenerate model pairs  $N_2$  depends on the distance in signature space  $\Delta S$ ; if signature space is effectively  $D_{\text{sig}}$  dimensional we expect

$$N_2 \sim (\Delta S)^{D_{\text{sig}}}. \quad (7)$$

Now, the precise definition of  $\Delta S$  requires some care. If we take the definition from section 4.3 and fit to  $N_2$ , we find in figure 11 that

$$N_2 \sim \begin{cases} (\Delta S)^{9.2} & \text{near } (\Delta S)^2 = 0.3 \\ (\Delta S)^{14.2} & \text{near } (\Delta S)^2 = 0.6 \end{cases}, \quad (8)$$

suggesting that the dimensionality of signature space in the vicinity of degenerate pairs is 9 to 14 dimensional.

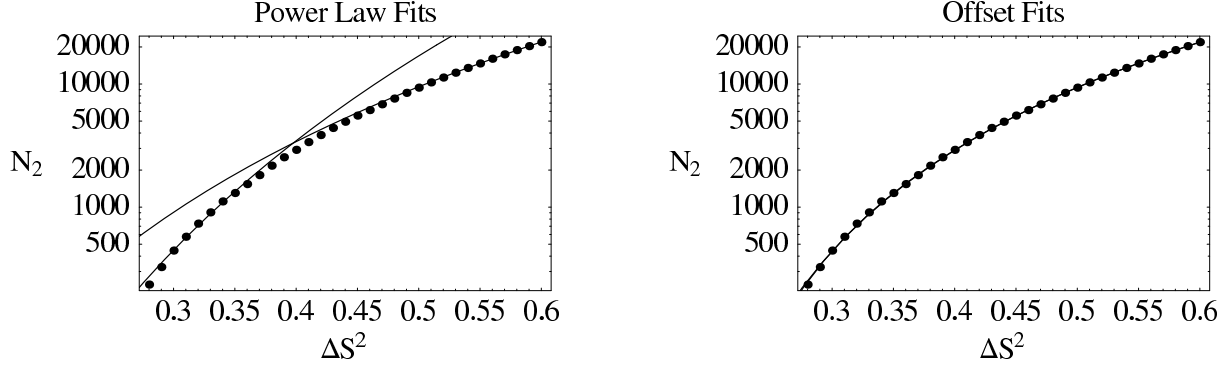


Figure 11: Dimensionality of signature space.  $(\Delta S)^2 = 0.285$  corresponds to statistical fluctuations, and the maximum value of  $(\Delta S)^2$  between pairs of models is  $\Delta S^2 \gtrsim 600$ , well off these plots. On the left plot, we fit to the power law  $N_2 \sim (\Delta S)^{D_{\text{sig}}}$  with exponents  $D_{\text{sig}} \sim 9$  and  $14$ . On the right plot, we take into account the possibility of an offset value  $\Delta S_0$ , yielding  $D_{\text{sig}} \sim 5$  or  $6$  (both curves are shown overlapping). In either case, we see that the effective dimensionality of signature space is much smaller than the dimensionality of parameter space, giving another justification for degeneracies.

Still, the fact that  $N_2$  does not seem to follow a simple power law in  $\Delta S$  indicates that  $\Delta S$  may not be the best measure of distances in signature space. In particular, even simulating the same model repeatedly gives some finite value of  $\Delta S$ , so one might guess that for a signature space of dimension  $D_{\text{sig}}$ :

$$N_2 \sim (\Delta S - \Delta S_0)^{D_{\text{sig}}} \quad \text{or} \quad N_2 \sim \left( \sqrt{\Delta S^2 - \Delta S_0^2} \right)^{D_{\text{sig}}}. \quad (9)$$

In figure 11, we see that this hypothesis is valid over a wide range of signature values, simultaneously giving good fits to<sup>4</sup>

$$N_2 \sim \left( \sqrt{(\Delta S)^2 - (0.42)^2} \right)^{6.2} \quad \text{and} \quad N_2 \sim (\Delta S - 0.39)^{4.4}. \quad (10)$$

These fits suggest that the true dimensionality of signature space is  $D_{\text{sig}} \sim 5$  or  $6$ , less than the number of MSSM parameters that we are varying. This makes it clear that in order to further break degeneracies, it is not enough to add a few extra signatures; one must add signals that are sufficiently orthogonal to the existing ones to increase the effective dimensionality of signature space.

Ideally, we could figure out what the 5 or 6 independent signatures are in a statistical sense by doing a multivariate regression on our LHC signatures. Unfortunately, it is computational

---

<sup>4</sup>The number  $\Delta S_0 = 0.42$  or  $0.39$  is interesting, because it is around the minimum  $\Delta S$  between identical models run with different random number seeds.

difficult to do such a regression on a 1808 dimensional signature space. Moreover, we expect at least some of the independent signature directions to change depending on the specifics of the MSSM spectrum.

### 3 Our Picture of the Inverse Map

The existence of degeneracies and cliffs substantiates the rough picture of the inverse map we suggested in figure 3 consisting of a number of small islands spread out over a large region in parameter space. The small size of the islands is reflected in the existence of cliffs, indicating that LHC observables are indeed sensitive to small parameter changes. The existence of many islands far apart in parameter space is substantiated by the presence of degeneracies.

Note that the figure assumes that the islands are “point-like” in parameter space. We actually don’t know that this is the case—they may be higher-dimensional manifold like tubes or sheets in parameter space. Indeed, if there are obvious flat directions in parameter space where for instance a particle is sufficiently decoupled as to play little role in the signatures, these would show up as higher-dimensional objects in the inverse map. All we can say with confidence from our analysis of cliffs is that the islands are not space-filling and constitute a small part of the total volume of the inverse map from a given signature.

The degeneracies have simple physical interpretations as shown in figure 12. As is common in hadron collider phenomenology, the cleanest handle on new physics often comes from looking at leptons. In SUSY models where sleptons are not copiously produced in a long SUSY cascade decay chain, the leptons dominantly come from  $W$ s and  $Z$ s produced in electroweak-ino cascade decays. In this case, we find large ambiguities in the spectrum of the remaining electroweak superpartners. Two models can have identical LHC signals by having “flippers” where electroweak-ino mass eigenvalues are fixed but with different eigenstates, “sliders” where the electroweak-ino spectrum is moved up or down keeping mass differences fixed, and “squeezers” where the information of some of the electroweak-inos is hidden because the mass splittings are small enough that the leptons in the decay products are too soft to be seen. We will discuss these degeneracy classes further in section 5.

Of course, the changes in the electroweak-ino sector are accompanied by suitable changes in the colored superparticle spectrum to match rates and other kinematical distributions between the models. The number of degeneracies for a given model arising in this way is of order 10 to 100. As we show in section 7, when sleptons are forced to be present in the cascade decays, there are more leptons in final states and the degeneracies virtually

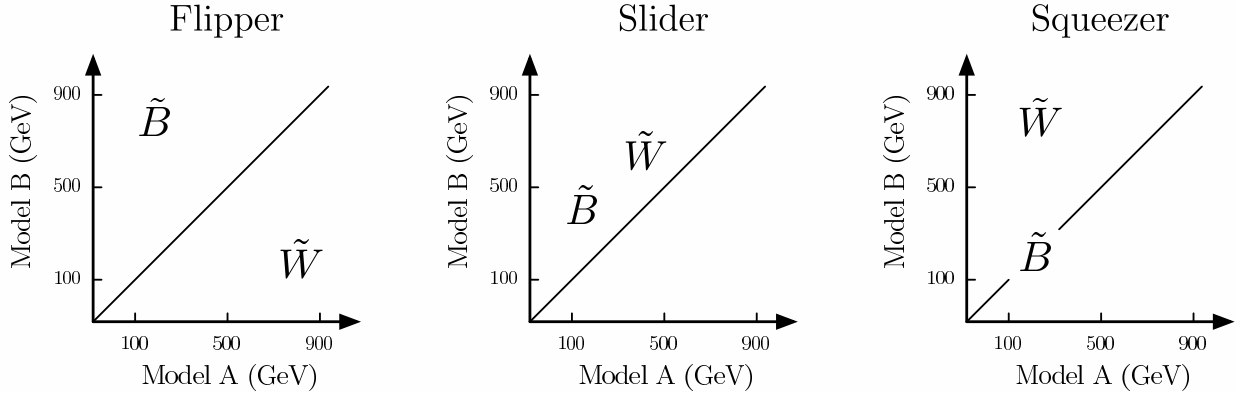


Figure 12: Dominant Degeneracies: Flippers, Sliders, and Squeezers. When scanning over the general MSSM, sleptons are generically decoupled, therefore important leptonic handles on the electroweak-ino spectrum are lost. This allows for three major classes of degeneracies. In a “flipper”, the identity of an electroweak-ino is changed while the mass eigenstates are fixed. In a “slider”, the entire spectrum is shifted while fixing mass differences. In a “squeezer”, a low-energy eigenstate is hidden because the decay products between adjacent mass eigenstates are soft. In the above cartoons, “ $\tilde{B}$ ” and “ $\tilde{W}$ ” can stand for a bino, a wino, or a higgsino.

disappear, although there may still be an ambiguity in swapping the left- and right-handed sparticle spectrum. But in the general case, our estimate of the number of degeneracies is as interesting as it could have been—the number is not one (*i.e.* there certainly *are* degeneracies) but nor is it  $10^6$ . Therefore while the existence of degeneracies represents a challenge, it is one that can likely be overcome by devising clever new observables to eliminate them. This would allow us to determine essentially *all* important aspects of SUSY physics with LHC data.

## 4 Details of Our Study

Even though the birthday problem has reduced the number of models to simulate from  $m \sim N$  to  $m \sim \sqrt{N}$ , the number  $N$  of experimentally distinguishable possibilities at the LHC is still quite large, and there a number of compromises one must make when comparing a large number of different models.

The first compromise is on the amount of data we can generate. For gluino masses around 600 GeV, there are around  $10^7$  SUSY events at an integrated luminosity of  $10 \text{ fb}^{-1}$ . Even without including the effect of initial state radiation and multiple interactions, it takes a fast

CPU over one hour to simulate that many events, and a simplified version of the event record is roughly 50 megabytes in size. Most previous collider studies assume that the LHC will achieve an integrated luminosity of  $300 \text{ fb}^{-1}$ , but it is simply impractical for us to generate, store, and analyze that much data for a large number of models. Therefore, we only generate  $10 \text{ fb}^{-1}$  of data for each model and force all colored particles to be heavier than  $600 \text{ GeV}$ . While the constraint of heavy colored particles was necessitated by computational limitations, there are independent reasons for making this choice. The characteristic signature of SUSY at the LHC is hard jets plus missing transverse energy, so while the cross section for SUSY increases as the gluinos and squarks get lighter, the jets from SUSY cascades get softer, making it more difficult to identify a pure sample of SUSY events.

The second compromise is on standard model background. While it is certainly possible to estimate the effect of standard model background on  $10 \text{ fb}^{-1}$  of data, the focus of this paper is not on separating SUSY signals from standard model background but on distinguishing between different SUSY models. At  $300 \text{ fb}^{-1}$ , one can make hard cuts and still maintain decent statistical significance of leptonic signatures, but this is difficult at  $10 \text{ fb}^{-1}$ . Therefore, we ignore standard model background in this study except as a guide for defining reasonable cuts and triggers.

This is simultaneously an optimistic and pessimistic choice, because by ignoring standard model background we are inflating the statistical significance of our small data sample, but by ignoring the effect of higher luminosity we lose access to rare processes that may give important clues in deciphering the data. We emphasize that both of these compromises are not intrinsic limitations, but are dictated by our current computing resources.

## 4.1 LHC Observables

Broadly defined, LHC data is anything that can be measured with an ATLAS- or CMS-like detector with delivered luminosity. To simulate  $10 \text{ fb}^{-1}$  of LHC data, we use PYTHIA [41] to generate parton level interactions and hadron showering and pipe PYTHIA output to a modified version of the CDF fast detector simulator PGS written by John Conway [42]. This modified version was developed by Steve Mrenna and approximates an ATLAS- or CMS-like detector. PGS yields reasonable efficiencies and fake rates and includes the effect of energy smearing.

We use a simplified output from PGS for our study, namely a list of objects in each event labeled by their identity (photon, electron, muon, hadronic tau, jet, b-tagged jet, missing  $E_T$ ) and their four-vector. Leptonic objects are also labeled by their charges. Using this

information, one can construct almost any LHC signature imaginable. Of course, when real data from the LHC arrives, various different techniques will be used to isolate, verify, and make measurements on samples. Because we are ignoring standard model background in our analysis, our goal is to choose a set of observables that are sensitive to MSSM parameters but which are sufficiently inclusive to be useful over a wide range of parameter values. Note that we make no attempt to interpret any of our signatures in terms of cross sections, branching ratios, or mass differences in the underlying model; instead, we simply compare raw signature values between different models.

While we are not including standard model background, initial state radiation, or multiple interactions in our analysis, in appendix B, we select cuts and triggers in a way that is aware of the challenges they pose. We will focus on events with 2 or more jets plus large missing transverse momenta, for while jet-veto signatures from direct production of electroweak-inos can sometimes be important, the standard model background is generically too large for the parameter region we scan.

The complete list of the signatures we use is given in appendix B. There are two different types of signatures we consider, counting signatures and kinematic histograms. Counting signatures give the number of events that pass a certain set of criteria. Because getting an accurate measurement of  $\sigma_{SUSY}$  is very difficult at the LHC, we only include one signature that counts the total number of SUSY events that pass the above cuts; all other counting signatures are given as ratios. The two types of kinematic histograms we generate are effective mass<sup>5</sup> and invariant mass for various different objects in events:

$$m_{\text{eff}} = \sum_a P_T^a, \quad m_{\text{inv}}^2 = \left( \sum_a p_\mu^a \right)^2. \quad (11)$$

We use a quantile method to define signatures for all of the kinematical distributions. The entries in a distribution are organized into bins of variable width such that each bin contain the same number of entries. For example, a decile distribution has ten bins which each contain 10% of the total entries. The signatures for a distribution are given by the boundaries of the bins, with no signature stored for the upper or lower boundaries of the total distribution. Therefore a distribution split into deciles has 9 signatures associated with it. Note that using the quantile method, the information of a distribution is in the positions of the bins, rather than the content of each bin.

Our adoption of the quantile method is dictated by the necessity of defining distribution observables which are applicable to a wide variety of models with very different mass spectra.

---

<sup>5</sup>In other contexts, “effective mass” means the  $P_T$  sum over missing energy and the four hardest jets. In this paper, we use effective mass to mean any  $P_T$  sum over any number of objects.

The traditional histogram method of fixed bin size is not practical here since we would have to include histograms with large energy ranges and with many different bins. Because different parts of the histogram would be populated by different models, we would either be forced to store a large number of redundant signatures or make the bin size so large that important kinematic information could be lost. The quantile method resolves this problem by converting distributions into a small number of easy-to-use inclusive observables.

In the SUSY literature, there is a large focus on endpoints and edges in kinematic distributions as ways of constraining mass differences between different SUSY particles [33, 34, 35, 37]. While it is difficult to teach a computer how to generically find an edge/endpoint (and assign appropriate error bars), the quantile method of describing histograms captures most of the statistically significant information in a kinematic distribution. So even though there is not a separate signature corresponding to an edge/endpoint measurement, the edge/endpoint will be well constrained by the requirement that all of the quantiles for the histogram match.

## 4.2 The Scanned Parameter Space

LHC signatures are mainly sensitive to mass parameters for the particles which either have large production cross sections or are important links in cascade decays. Considering both the strong constraint from FCNC measurements and the lack of sensitivity in LHC observables included in the current study, we have imposed universality conditions on the masses of the first two generations of scalar fermions. On the other hand, third generation mass parameters are treated as independent. Flavor off-diagonal entries in the sfermion mass matrices are assumed to vanish. Left- and right-handed sfermions are allowed to have independent mass parameters.

We scan  $\tan\beta$  and the following 14 SUSY mass parameters:

$$\begin{aligned}
 \text{Inos :} & \quad M_1, M_2, M_3, \mu \\
 \text{Squarks :} & \quad m_{\tilde{Q}_{1,2}}, m_{\tilde{U}_{1,2}}, m_{\tilde{D}_{1,2}}, m_{\tilde{Q}_3}, m_{\tilde{t}_R}, m_{\tilde{b}_R} \\
 \text{Sleptons :} & \quad m_{\tilde{L}_{1,2}}, m_{\tilde{E}_{1,2}}, m_{\tilde{L}_3}, m_{\tilde{\tau}_R}
 \end{aligned}$$

We have separated left- and right-handed sfermions. The soft masses for the first two generations are universal. For right-handed squarks, the up- and down-types are varied independently. In order to constrain the Higgs sector, we take the mass of the pseudoscalar Higgs to be 850 GeV. We also fix the third generation squark  $A$ -terms at 800 GeV.

We scan the parameter space by randomly sampling the 15 dimensional parameter space.

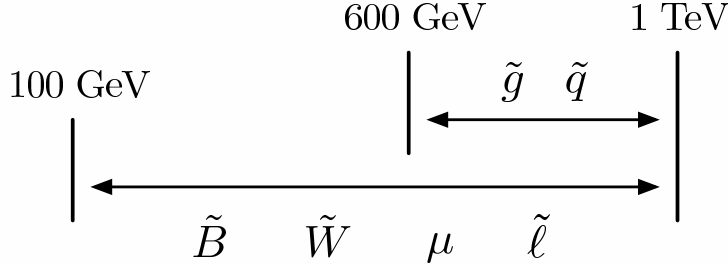


Figure 13: Parameter Ranges for our General Scan. The gluino and the six squark masses are randomly sampled between 600 GeV and 1 TeV. The three electroweak-ino and the four slepton masses are randomly sampled between 100 GeV and 1 TeV. The value of  $\tan\beta$  is scanned between 2 and 50.

We sample all mass parameters uniformly in mass value, and scan  $\tan\beta$  uniformly from 2 to 50. The range of mass parameters in our general scan is shown in figure 13.

Note that we do not enforce the mass of the Higgs to be above the experimental bound. The reason is that in order to get a heavy enough Higgs in the MSSM, we would be forced into a small region of parameter space with large  $\tan\beta$  and large stop masses. Because the LHC signatures of SUSY are dominated by colored particles and are largely independent of the Higgs sector, we do not want to limit the kinds of allowed SUSY signatures by placing artificial restrictions on the SUSY parameters, especially because the Higgs mass may be lifted due to an extended Higgs sector.

We also impose a non-decoupling criterion to minimize the number of flat directions in the map from parameter space to signature space. Let  $m_{\text{slepton}}^{\text{max}}$  be the heaviest slepton soft mass,  $m_{\text{ino}}^{\text{max}}$  be the heaviest electroweak-ino mass parameter ( $M_1$ ,  $M_2$ , or  $\mu$ ), and let  $m_{\text{color}}^{\text{max}}$  be the soft mass or mass parameter for the heaviest color-charged particle. We demand:

$$m_{\text{slepton}}^{\text{max}} < m_{\text{ino}}^{\text{max}} + 50 \text{ GeV} < m_{\text{color}}^{\text{max}} + 100 \text{ GeV}. \quad (12)$$

The purpose of the non-decoupling criterion was to ensure that apart from the 50 GeV buffer, there was always a kinematically allowed cascade decay involving sleptons in the sample. However, this non-decoupling criterion in no way guarantees that sleptons will play a dominant role in the decay chain. As we discuss more in sections 5 and 7, scanning over the MSSM, the total production rate for sleptons from cascade decays is generically small.

### 4.3 Comparing Models

The most statistically sound method for testing whether a set of LHC observables matches a given model is to generate an “infinite” statistics sample of that model, and do a  $\chi^2$  test to estimate the likelihood that the LHC data matches that model. Because we are focusing on testing whether there are SUSY models that share the same signatures with  $10 \text{ fb}^{-1}$  of data, we only need to find a measure of the difference between data sets, and then establish a threshold below which models are considered degenerate.

We define a  $\chi^2$ -like variable to measure the difference between two models

$$(\Delta S_{AB})^2 = \frac{1}{n_{\text{sig}}} \sum_i \left( \frac{s_i^A - s_i^B}{\sigma_i^{AB}} \right)^2, \quad (13)$$

where  $s_i^A$  ( $s_i^B$ ) is the value of the  $i$ -th signature for model  $A$  ( $B$ ),  $\sigma_i^{AB}$  is the error bar assigned between models  $A$  and  $B$  for the  $i$ -th signature, and the sum over  $i$  runs over  $n_{\text{sig}}$  relevant signatures. A relevant signature is one that would not artificially reduce  $\Delta S_{AB}$  because of low statistics. We define a relevant signature to be one for which the error bar  $\sigma_i^{AB}$  is smaller than both  $s_i^A$  and  $s_i^B$  or for which  $|s_i^A - s_i^B| > \sigma_i^{AB}$ . The value of  $\sigma_i^{AB}$  is given by

$$\sigma_i^{AB} = \sqrt{(\delta_{\text{stat}} s_i^A)^2 + (\delta_{\text{stat}} s_i^B)^2 + \left( f_i \frac{s_i^A + s_i^B}{2} \right)^2}, \quad (14)$$

where the statistical errors  $\delta_{\text{stat}}$  are described in Appendix C, and  $f_i$  is an additional fractional error parameter that could be used to estimate standard model background errors. For our study we take  $f_i = .01$  for every signature except the total number of SUSY events, for which we take  $f = .15$ .

In order to figure out the value of  $(\Delta S_{AB})^2$  that defines the typical size of statistical fluctuations, we ran a subset of our models again with a different random number seed and calculated the  $\Delta S^2$  values between duplicated models. We define the cutoff as the 95th percentile of these  $\Delta S^2$  values, yielding  $(\Delta S_{95\text{th}})^2 = 0.285$ .

One concern in using a  $\chi^2$ -like variable to distinguishing models is that it does not account for the fact that if one signature differs by a large ( $> 5\sigma$ ) amount, the overall  $\chi^2$  can be still be very small. This is especially a concern in our case where the total number of signatures—1808—is very large, and we discuss this concern in more detail in section 6. One could try using the condition that models are considered the same only if every signature is within  $5\sigma$ , however, using this criteria would force us to reject identical models generated with different random number seeds where one or two signatures differ by more than  $5\sigma$  because of a large statistical fluctuation. Another deficiency of a  $\chi^2$ -like variable is that it does not account

for the fact that certain signatures are better than others at distinguishing between models. However, in trying to develop an optimally weighted  $(\Delta S_{AB})^2$  variable, we have found no effective weighting strategy which will enhance the statistical significance of the difference between degenerate models.

In order to quantify the distance between two models in parameter space, we define  $\Delta P^2$  as:

$$(\Delta P_{AB})^2 = \frac{1}{n_{\text{para}}} \sum_i \left( \frac{p_i^A - p_i^B}{\bar{p}_i^{AB}} \right)^2, \quad \bar{p}_i^{AB} = \frac{p_i^A + p_i^B}{2} \quad (15)$$

where  $p_i^A$  ( $p_i^B$ ) is the value of the  $i$ -th parameter for model  $A$  ( $B$ ) and the sum runs over  $n_{\text{para}}$  parameters. Roughly speaking,  $\Delta P^2$  gives the quadrature average of the percentage difference between model parameters. Depending on the context, this sum can run over all the parameters or just a subset.

## 5 Characterizing the Degeneracies

The pigeonhole principle argument tells us that there must be degeneracies, but it does not tell us what the degeneracies actually are. And it is clearly challenging to find an algorithm to systematically find all degeneracies associated with a given model, precisely because they are not “close” to each other and there is no obvious way to continuously travel between degenerate pairs. Plus, the existence of cliffs shows that it would be difficult to find local minima in signature distance because of the strong sensitivity of LHC observables to the SUSY parameters. Nonetheless, as we will see the degeneracies have rather simple characterizations, and understanding these will help in devising strategies for breaking the degeneracies with more signatures.

The first important point is that the gross properties of the colored superpartner spectrum—the masses of the gluinos and squarks—are largely determined by our signals. In figure 14 we examine the  $(\Delta S^2, \Delta P^2)$  plot where  $\Delta P^2$  only includes the gluino mass separation. This perfectly resembles the “best of all possible worlds” plot from figure 5—it is beautifully triangular and there are no degeneracies for gluino masses. The analogous plots for squarks are also shown in figure 14. Note that there is greater variation in  $\Delta P^2$  for small  $\Delta S^2$ , indicating that LHC observables are not as sensitive to individual squark masses as gluino masses. One of the reasons why the variations in squark masses are small is that squarks are scanned in a small range compared to sleptons and electroweak-inos. However, the mass of the lightest squark is still well constrained, suggesting that the jet signatures fix some overall scale for the squarks but not their flavor or handedness.

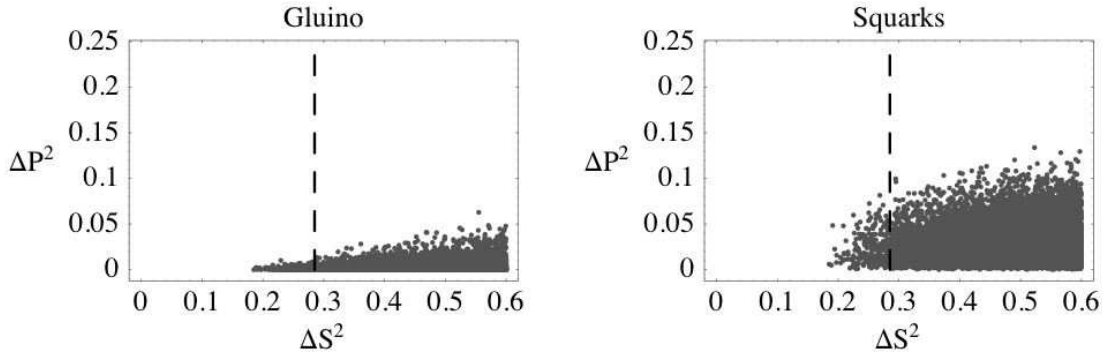


Figure 14: A  $(\Delta S^2, \Delta P^2)$  plot for gluinos and squarks, where again  $\Delta P^2 \sim 0.01$  roughly corresponds to 10% accuracy in the desired parameters. We see that the maximum variation in gluino and squark masses is roughly 10% and 40%, respectively. While not shown in these plots, the variation in the mass of the lightest squark (regardless of identity) never exceeds  $\sim 15\%$ . In the plot for squarks, the variation of the mass parameters is calculated as the average variation of individual squark mass parameters.

The plot for slepton masses in figure 15 is very different. Note that there is a continuous spread of slepton masses at small  $\Delta S^2$ . Evidently we are not particularly sensitive to the slepton mass over large ranges of parameter space; this is unsurprising because sleptons are not copiously produced in cascade decays in most of the regions of parameter space we have simulated. Similarly,  $\tan \beta$  is generically unconstrained, because while the higgsino couplings are controlled by  $\tan \beta$ , movement of the third generation squarks can often compensate for changes in the branching ratio to higgsinos.

The situation is different still with the electroweak-inos, as can be seen from figure 16. Here we see dramatic evidence for the existence of degeneracies—at small  $\Delta S^2$ , the plot has two branches with small and large  $\Delta P^2$ . This is strong evidence for discrete ambiguities in the determination of electroweak-ino parameters.

The existence of degeneracies in the electroweak-ino sector may seem counter-intuitive. After all, the electroweak-ino sector in the MSSM is made of particles from different representations of  $SU(2)_L \times U(1)_Y$ . Therefore, they couple very differently to matter multiplets and to standard model gauge bosons. For example, the bino will couple to both left-handed and right-handed states, while the wino only has left-handed couplings. The wino and the higgsino have both charged and neutral states—approximately degenerate in mass—as part of the same multiplet, while the bino only has a neutral state.

Therefore, one might expect that LHC signature should be very sensitive to not only the masses, but also the identities of the electroweak-inos. Indeed, two otherwise identical mod-

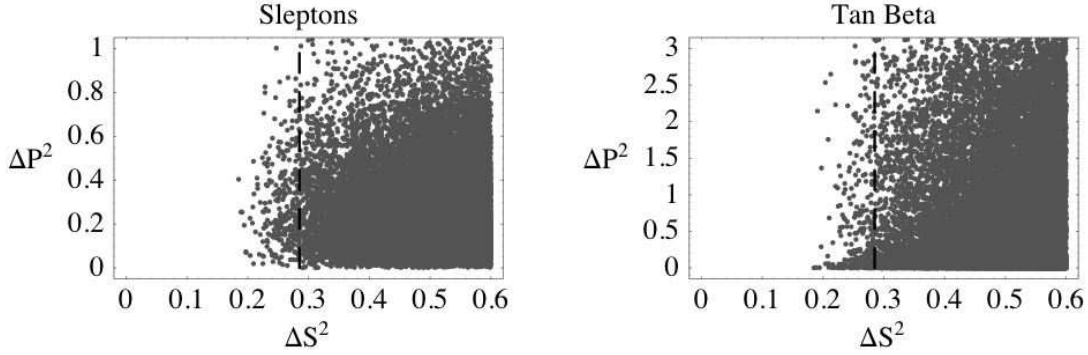


Figure 15: A  $(\Delta S^2, \Delta P^2)$  plot for sleptons and  $\tan\beta$ . We see that none of these parameters are particularly well constrained. The variation of the slepton mass parameters is the average variation of individual slepton masses.

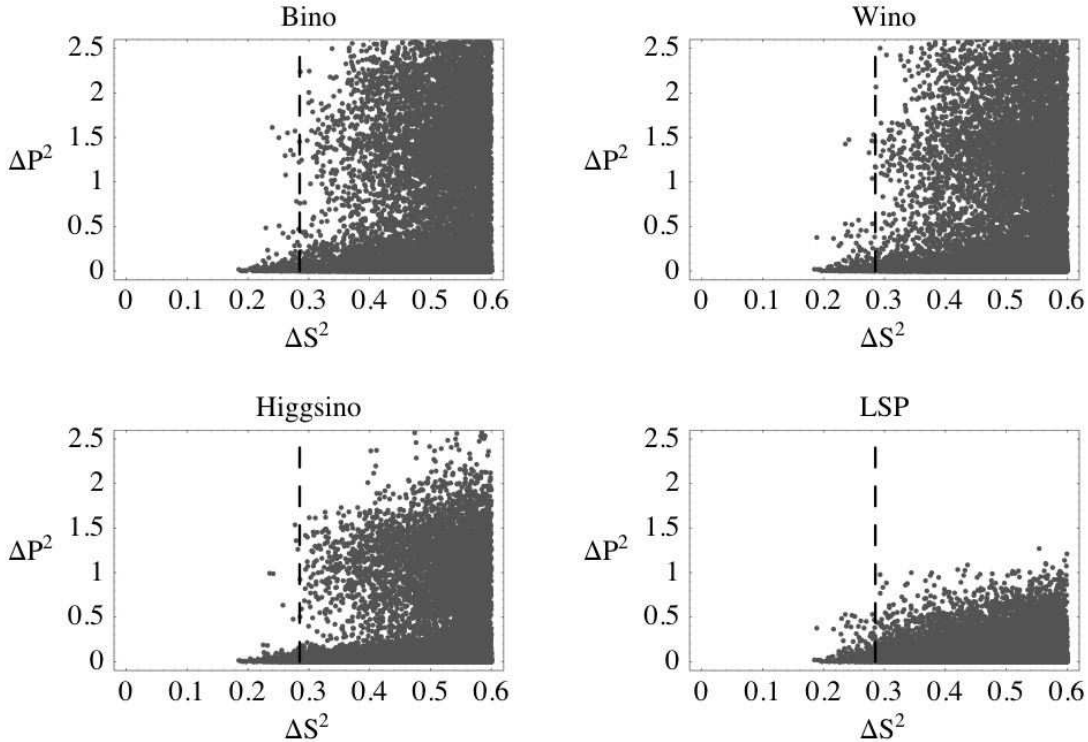


Figure 16: A  $(\Delta S^2, \Delta P^2)$  plot for electroweak-inos. In these plots we see the presence of two regions at small  $\Delta S^2$ . There is a lower triangular region, in which the electroweak-inos are constrained to at most 20% - 40% variation. Then there is an upper region where the electroweak-ino masses appear unconstrained. This indicates the presence of discrete choices in the electroweak-ino spectrum. Note that the mass of the LSP mass is much better constrained than the mass of the individual electroweak-inos, showing that LHC signatures are sensitive to mass eigenvalues but not mass eigenvectors.

els with different electroweak-ino mass parameters produce quite different LHC signatures. However, our key observation is that such changes of the electroweak-ino mass parameters can sometimes be compensated by changes of other soft parameters.

In general, we can attribute the existence of degeneracies to the following facts. First, in principle, the identity of final state quarks from SUSY decay chains carries a lot of the information about various intermediate superpartner states. On the other hand, except for the partial flavor tag of the third generation, all other information of the quantum numbers of final state quarks are lost. Second, most of the kinematical observables, such as  $P_T$ , are only sensitive to the mass splitting of the superpartners, not their identities. Third, there are large region of parameter space where the electroweak-inos have nearly identical decay modes, hence very similar signatures. For example, as long as the mass splitting between the electroweak-inos is greater than  $m_W$  and sleptons are decoupled, the dominant decay mode of a chargino is almost always  $\chi^\pm \rightarrow W^\pm + \text{LSP}$ , relatively insensitive to the mixings of two chargino states. Finally, we do expect to get a better handle on the identity of the electroweak-inos if the decays through on-shell sleptons have significant branching ratios, due to the fact that leptonic signatures typically carry much more information comparing to jet signatures. On the other hand, without any theoretical preference, this is a very special corner of the MSSM parameter space.

Notice that overall event rate, while the most statistically significant observable for measuring mass scales of colored particles, is not a sensitive observable to the more subtle structure of degeneracies involving electroweak-inos and sleptons. Nor is it sensitive to individual movements of squark mass parameters, as long as some rough overall squark mass scale is fixed.

The electroweak-ino degeneracies can be characterized in a number of simple ways, which we describe in the following subsections.

## 5.1 Flippers

Flippers are probably the most dramatic example of degeneracies in the electroweak-ino sector. In this case, although the mass eigenvalues of two sets of electroweak-inos remain approximately the same, the identities of two members of them are swapped. We observe that it is possible to make such a swap without significantly changing the signatures by adjusting somewhat the other SUSY mass parameters at the same time, such as left- and right-handed sfermions masses.

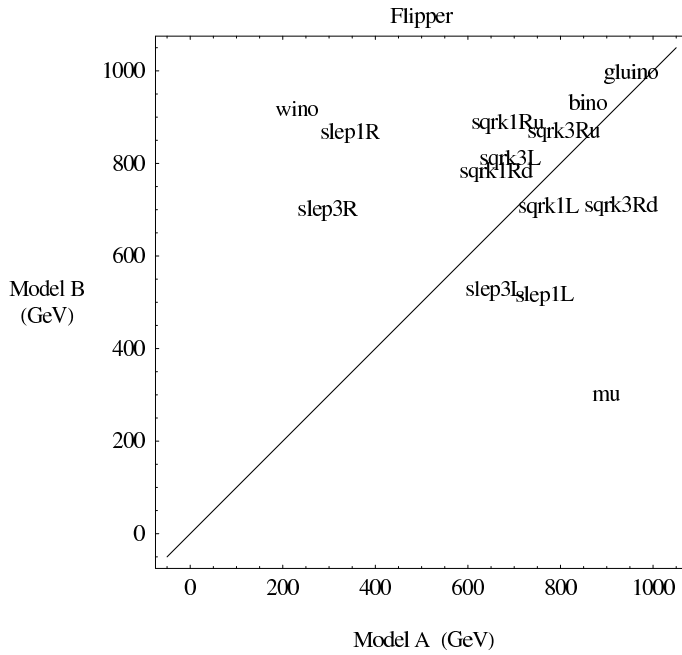


Figure 17: An example of a Flipper, where the masses of the electroweak-inos stay roughly fixed but their identity changes. In this example a wino LSP is replaced by a higgsino LSP.

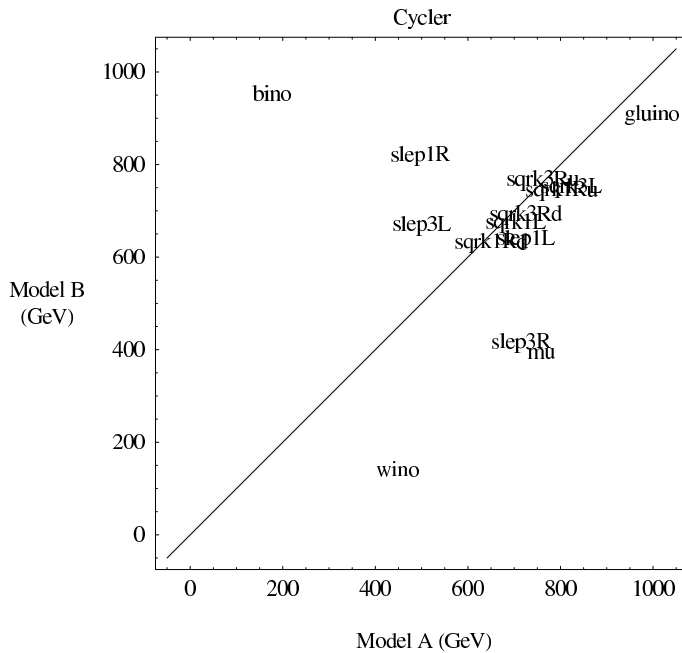


Figure 18: An extreme example of a flipper is a Cycler, where the electroweak-ino identities undergo a cyclic permutation. In model A,  $\tilde{B} < \tilde{W} < \mu$ , whereas in model B,  $\tilde{W} < \mu < \tilde{B}$ .

A simple example of a flipper is shown in figure 17. In this pair of models, although the LSPs have approximately the same mass, their identities are wino and higgsino, respectively. Besides the LSP, other electroweak-inos are at most barely in the decay chain, because of the suppressions either from phase space or from an off-shell squark. The dominant channel of decay of gluino and squarks are directly to jets and LSP. Since we do not measure the charge of the jet, such signals reveal very little about the identity of the LSP. Notice also that the masses of the other squarks and sleptons moved in this example, compensating possible differences from a simple swap of the wino and higgsino.

Another more dramatic example of a flipper—a “cyclor”—is shown in figure 18. In this case, the identities of the three electroweak-inos in the degenerate models differ by a cyclic permutation. In each of these two models, there are two electroweak-ino states lighter than the gluino and squarks, and hence both are present in the decay chain. On the other hand, in the absence of a significant slepton branching ratio, the decay between the two electroweak-ino states is dominated by  $W$ s,  $Z$ s and Higgses, and Higgs information is always less significant due to backgrounds, trigger bias, and tagging efficiency. Therefore, again, the lower stage of decay chain, which is the most relevant for understanding the electroweak-inos, are not very telling in this case. We will discuss this example in more detail in section 6.

## 5.2 Sliders

Due to the existence of a neutral massive particle escaping the detector, most of the LHC observables for SUSY are only sensitive to mass differences. Therefore, we would expect that the signatures would not change significantly if we shifted the mass spectrum while holding mass differences fixed. Because we also use the total rate as one of the observables, we expect that we will not be able to change the parameters a lot this way. The slide in the spectrum will have to be somewhat uneven in different parameters as well.

An example of such a slider is shown in figure 19. The dominant production channel for these two models are gluinos. We see that the masses of a number of states change collectively in one direction, keeping the most important mass gaps, such as between gluino and the LSP, approximately fixed.

## 5.3 Squeezers

If the mass separation between the two states in the decay chain is very close, the decay processes between them will only generate very soft objects which are below detection threshold.

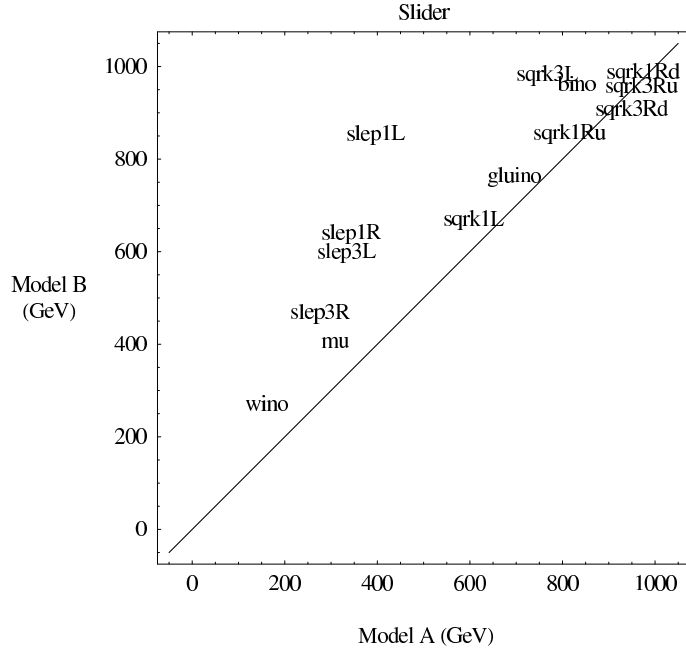


Figure 19: An example of a Slider, where the spectrum is shifted up, keeping the mass difference among the electroweak-inos and gluinos roughly fixed. In this case, the shift is about 100 GeV for the most relevant parameters.

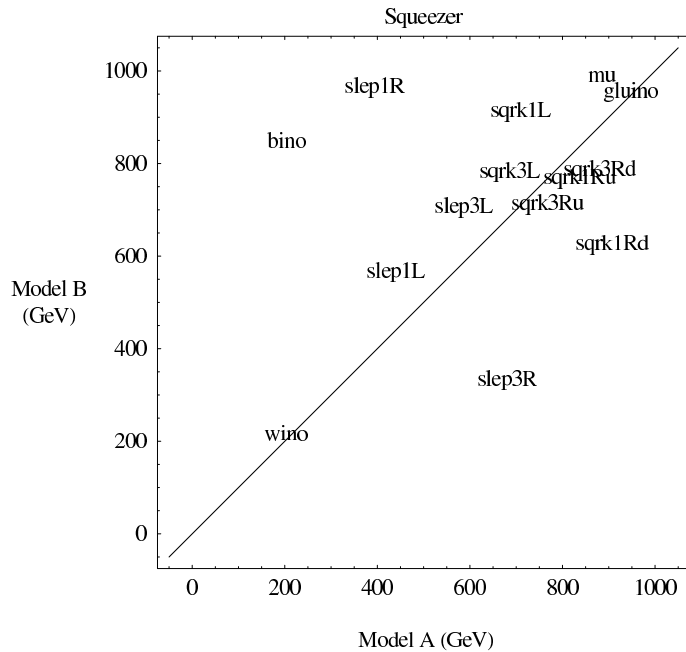


Figure 20: An example of a Squeezer, where the mass difference between electroweakinos is made small such that the decay products between adjacent states are too soft to detect. In this example, the LSP mass is fixed, but the number of neutralino states at low energies changes from 2 in model *A* to 1 in model *B*.

In this case, we expect to have little ability of telling them apart as different states.

One example of such a squeezer is shown in figure 20. In model *A*, a wino state is almost degenerate with a bino state, while in model *B*, only a wino state light with about the same mass. One would expect to be able to tell the difference between these two models since the lower lying states have different ratios of neutral and charge states. On the other hand, it turns out, due to the structure of other soft parameters in these two models, the dominant decay to the light states only contain jets. Therefore, because of the charge blindness of the jets, we lose information about the charge of the final states.

## 6 “Are There Really Degeneracies?”

Strictly speaking, we base our analysis and counting of degeneracies on a global  $\chi^2$ -like variable. It is well-known that doing a  $\chi^2$  fit with a large number of observables—1808 in our case—will be sometimes misleading. In particular, it is in principle possible that two models differ by a large amount in a few observables, hence are distinguishable, but can still have a small  $\Delta S^2$  difference and be mistakenly identified as a degenerate pair. This is certainly a valid concern, but we argue that this effect is not very important in our counting and characterization of degeneracies.

First of all, the limitations of a  $\chi^2$  fit are only apparent when there are a small number of observables that are dramatically different. The sort of situation that can arise is that two models agree on everything except one signature which is different by, say,  $10\sigma$ . However, this is not likely to happen in our study—from the analysis of section 2.5, we find that most of our observables are correlated and the actual number of independent signature is small. More specifically, if we assume there are  $\sim 10$  independent observables in the set used in this study, then if we compare two models and one signature is off by  $5\sigma$ , then we would generically expect 10% of all the observables to also show significant deviations, making it all but impossible for that pair of models to have a small enough  $\Delta S^2$  to be called degenerate.

We can also examine the degenerate examples we have found and check for such an effect. We can compare, for instance, the maximum deviation in the signatures with dileptons, with the same deviation from simulating the identical model with different random number seed. Dilepton signatures are chosen here since they have very little standard model background after cuts and a significant difference in them will definitely break the degeneracy.

In particular, we ask what fraction of the degenerate candidates in our database have at least one dilepton signature deviation greater than  $5\sigma$ , and whether that fraction is consistent

with statistical fluctuations. Out of the 283 pairs in the general scan within the strict criteria of  $\Delta S^2 < 0.285$ , 46 had some dilepton signal that differed by more than  $5\sigma$ , yielding a failure rate of 16%. But out of 2600 models run with different random number seeds, 611 had some dilepton signal greater than  $5\sigma$ , yielding a statistical expectation for a 23% failure rate. Therefore, we see that the failure rate is consistent with statistics, showing that generically our definition of  $\Delta S^2$  identifies true degeneracies.

We could do such a comparison in other classes of signatures as well, but such a comparison will be less meaningful for several reasons. Signatures with fewer leptons typically have much larger standard model background. Therefore, the statistical errors we have used in our study are not realistic. In particular, we expect only large and qualitative differences in these signatures to be useful in distinguishing SUSY models. At the same time, compared with dilepton signatures, it is much easier to make small changes in the soft parameters to obtain a better fit to zero or one lepton signatures. For example, a large deviation in the total number of SUSY events can be compensated by a very small change in the gluino mass with negligible effects on the other signatures.

To give a sense of how different the LHC observables are in a typical degenerate pair of models, we can look more closely at a specific example which has interesting swaps in electroweak-ino masses—the “cyclor” example shown in section 5.1. There is no significant difference in the dilepton signatures for the cyclor pair. Therefore, it is not at all obvious how we should distinguish them. This is also a pair of models where we do see some discrepancies in some of the other signatures, which are however unlikely to be useful to qualitatively distinguish the two models.

A set of typical observables for this pair are plotted in figure 21. Columns labeled by A and B are from the degenerate pair of models. Column C shows distributions from running model A again with a different random number seed, which provides a guide for the size of statistical fluctuations. Visually, we see that there is no difference in the counting of  $b$ -jets or in the  $M_{\text{eff}}$  distribution, despite the fact that those distributions showed some variations between models A and B ( $1\sigma$ – $3\sigma$ ). Except for the signatures we discuss below, all other counting signatures and distributions showed comparable or smaller deviations.

The shapes of the dielectron invariant mass distributions are somewhat different. On the other hand, the difference between models A and model B are at least as big as the difference between model A and model C, showing that at  $10 \text{ fb}^{-1}$ , there is not much information in these dilepton invariant mass distributions. Whether there could be some smoking gun in this distribution at  $300 \text{ fb}^{-1}$  is unknown.

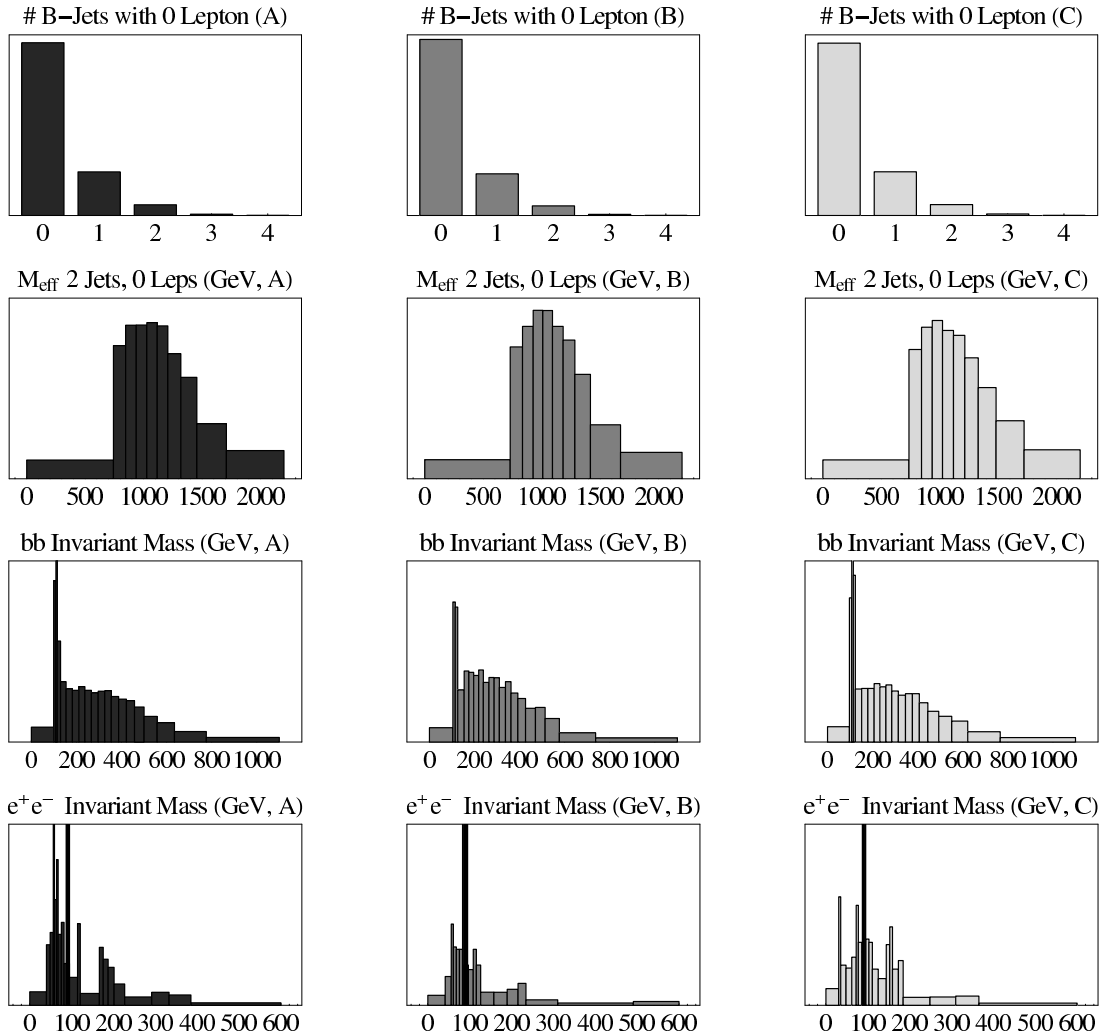


Figure 21: Example distributions from the “cyclor” example of figure 18. Model A and B are a degenerate pair, while model C has the same parameters as model A but was generated with a different random number seed. Note that histograms are plotted in quantiles—equally occupied bins of variable width. With the exception of lepton charge and total number of events as discussed in the text, all counting signatures have roughly the same variation among the three models as the  $b$ -jet counting example shown here. Similarly, all kinematic histograms have the same or smaller variation as the  $M_{\text{eff}}$  example. While the dielectron invariant mass distribution looks different between models A and B, it also looks different between models A and C, so we can ascribe such differences to statistical fluctuations. The main difference between models A and B is seen in the rate of Higgs production from the  $bb$  invariant mass distribution, though as we argue in the text, such a difference is washed out by  $t\bar{t}$  standard model background and also depends on the details of the Higgs sector, which we made no effort to control in our study.

One potential difference in these two models is the  $b\bar{b}$  invariant mass distribution. In both models, Higgs bosons are produced as part of the decay chain. In model A, Higgses are more copiously produced, and there is a  $4\sigma$  difference in the rate of Higgs production. On the other hand, it is very unlikely such a signature will be useful, even at high luminosity. First of all, at least with our cuts, such a deviation will not be visible once we include the standard model  $t\bar{t}$  background. Moreover, such a difference is highly sensitive to the details of Higgs sector. If there is a significant modification of Higgs sector of the MSSM, such as including a singlet in the possible decay product of the Higgs, this deviation will almost certainly be most less prominent.

The largest deviation in the observables between these two models is a somewhat large charge asymmetry in the single lepton signature, about 20%, corresponding to  $7\sigma$ – $8\sigma$  using only statistical error bars. However, distinguishing these two models based on this difference in single lepton signature will be very challenging due to the existence of large standard model background. At higher luminosity, one might expect the charge asymmetry to appear in trilepton events, but given the absence of sleptons in the decay chain, trilepton signatures will be relatively sparse.

Furthermore, the charge asymmetry is not necessarily a robust qualitative difference between these two scenarios either. The dominant contribution to such a difference comes from squark-gluino associated production, which is in turn very sensitive to small differences in squark masses. Because the overall rate of SUSY events between models A and B differ by  $4\sigma$  due to a 50 GeV shift in the gluino mass, we could fine-tune the gluino mass in one of the models to make the overall SUSY production rate more comparable, and such a fine-tuning (accompanied by other shifts in the squark sector) could alleviate the charge asymmetry without drastically modifying other observables.

The cyclor example is chosen here not because the pair has completely identical signatures, but because it exemplifies an interesting structure of degeneracy. The fact that two such drastically different models could come this close with observables extracted from only pure signal gives us the confidence that they are good representatives of a degenerate scenario.

Because of the ambiguity of the  $\chi^2$  analysis, there is no reason to believe that the best examples of degeneracies should be within the signature cut of  $\Delta S^2 = 0.285$ . There are pairs with somewhat larger signature separation and yet with no qualitative difference in any particular signature. The apparent difference in total  $\chi^2$  comes from adding up small deviations from a number of observables, which is expected due to the large number of

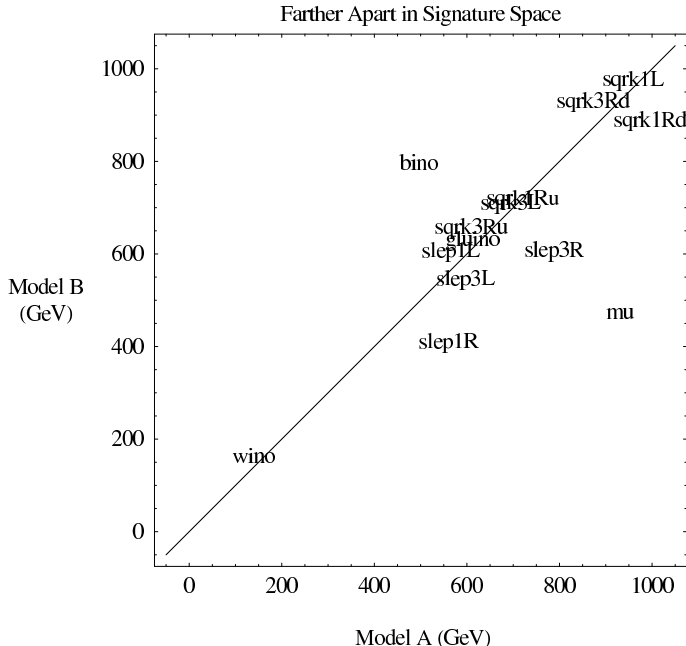


Figure 22: An example of a pair of models whose signature distance ( $\Delta S^2 = .457$ ) is larger than the cutoff defined in this paper for degenerate models. While these models can be distinguished by our  $\chi^2$  fit, it is possible that by slightly changing the parameters in this model, a robust degeneracy could be formed. This pair qualifies as a flipper, in that the identity of the second electroweak-ino is changed from a bino in model *A* to a higgsino in model *B*.

observables. Such pairs may actually be a better representative of a qualitative degeneracy, and we expect that nearby models in parameter space would form degenerate pairs satisfying a stricter degeneracy criteria.

Such an example is shown in figures 22 and 23. This pair of models is a flipper degeneracy where the second-lightest electroweak-ino changes from a bino to a higgsino. While there are many  $1\sigma$  variations in numerous signatures, there is no qualitative difference between these two models in any of the inclusive signatures. The most noticeable difference is an 8% difference in the inclusive one lepton counting, whose effect is somewhat visible on the plot in figure 23. There is also a 9% difference in the counting of 2 jet with no lepton events. Such deviations will almost certainly be swamped by large standard model background. There is no charge asymmetry in one lepton events, nor evidence for different rates of Higgs or  $Z$  production, nor any other potentially qualitatively different structure in all the other signatures. Such an example suggests that in the vicinity of pairs of models that lie a moderate signature distance apart, one could arrange robust degenerate pairs by making small parameter variations to smooth out  $1\sigma$  differences.

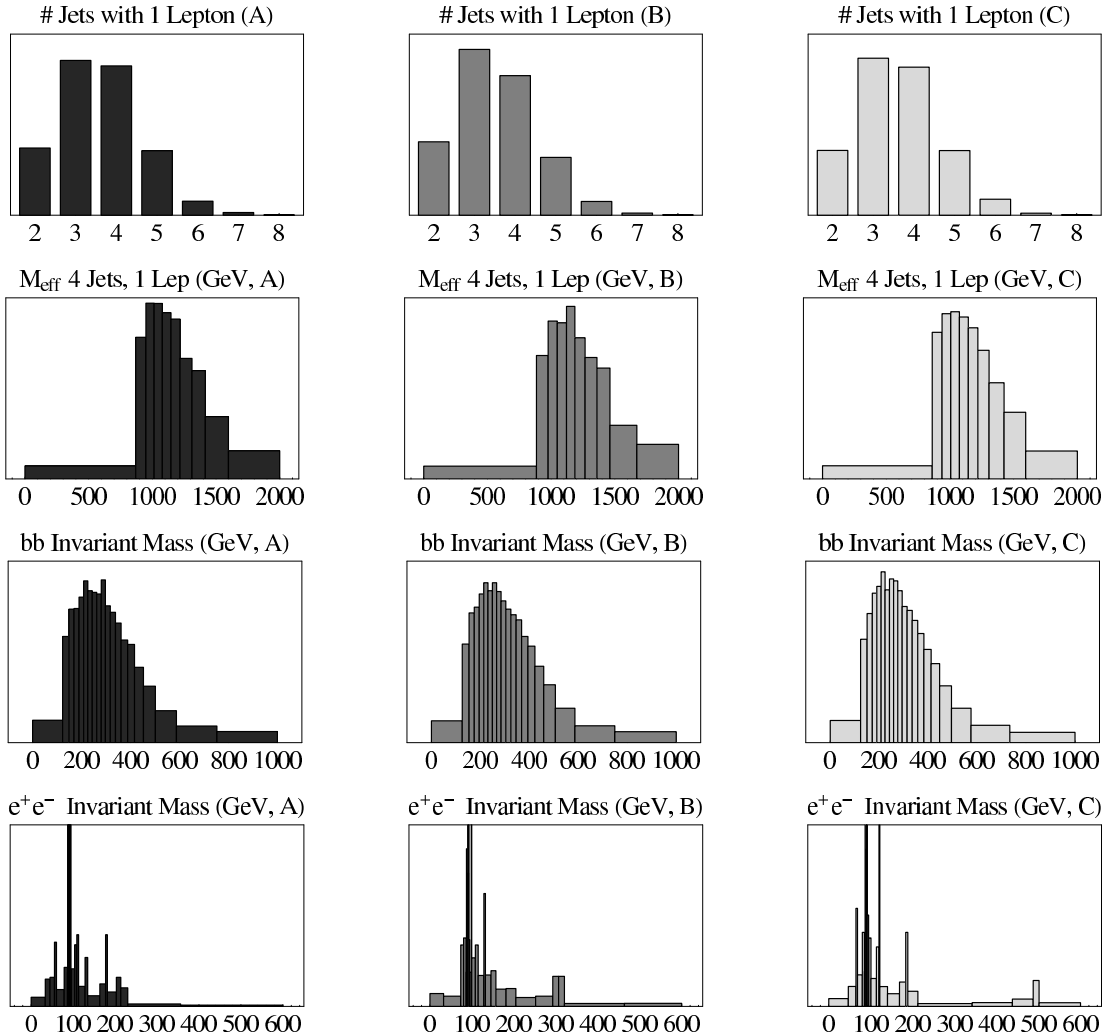


Figure 23: Example distributions from the pair of models in figure 22. Like figure 21, model *C* has the same parameters as model *A* but was generated with a different random number seed. The most noticeable difference in these plots is a slight imbalance in the number of 3 jet vs. 4 jet events with 1 lepton present. All of the other distributions are qualitatively similar between models *A*, *B* and *C*; a typical variation is shown for a  $M_{\text{eff}}$  plot. While a slight bump in the dielectron invariant mass distribution is present in model *B* at 300 GeV, the significance of such a feature is called into question by the presence of a similar bump in model *C* at 500 GeV which is entirely absent from model *A*, despite the fact that they share the same underlying parameters.

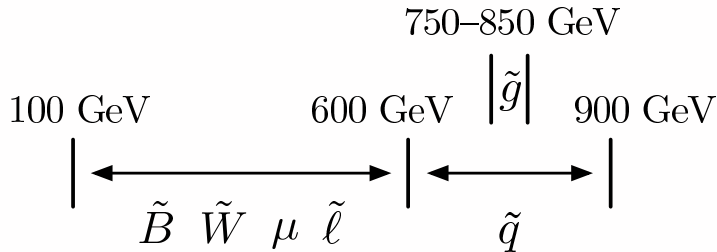


Figure 24: The parameter ranges for our dedicated cascade decay scan. Unlike the previous scan, we assume flavor universality for the sleptons and squarks, but we will still split left- and right-handed sfermions, and up- and down-type squarks. We force that the heaviest slepton is lighter than at least one electroweak-ino. As before,  $\tan \beta$  ranges from 2 to 50.

## 7 Sleptons and Long Cascade Decay Chains

Part of some people’s optimism about making precision measurements at the LHC comes from studying leptonic signatures. Not only is the standard model background smaller for events with hard jets and missing energy and hard leptons, but leptons, with their charge and flavor identified, carry much substantial information about the underlying processes. Moreover, the energy resolution on electrons and muons is much better than for jets. So while colored particles in SUSY guarantee that SUSY cross sections will be large at the LHC, it is leptons from cascade decays that are entrusted with constraining the SUSY spectrum.

In constrained models like mSUGRA or GMSB, we have reason to believe that slepton will be light, and therefore a reason to expect electroweak-ino-slepton-electroweak-ino cascade decays. Notice that the parameter region where we have a large slepton production in the decay chain is quite special. It certainly requires electroweak-inos, in particular those with large gaugino fractions, to be heavier than the first two generations of sleptons. At the same time, it also requires those inos to be light enough so that they are in the decay chain from gluinos and squarks. This set of requirements enforce a well-ordered mass spectrum from a general MSSM point of view.

In order to explore this special situation better, we have conducted a dedicated scan, as shown in figure 24, in which we enforce the existence of some long decay chains. In particular, the heaviest slepton is required to be lighter than at least one of the electroweak-inos. Also, we do not split the third generation of squarks and sleptons from the first two generations, with the idea that in most theoretical models with long cascade decays, there is usually some kind of flavor universality.

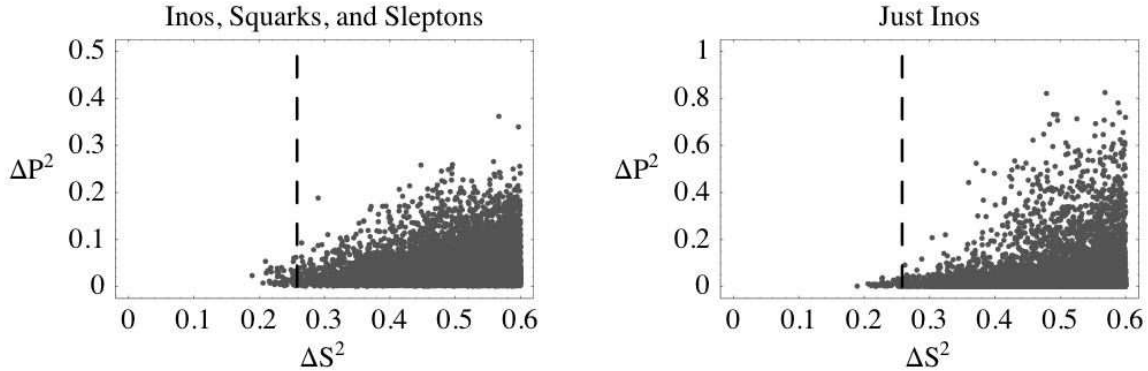


Figure 25: A  $(\Delta S^2, \Delta P^2)$  plot analogous to figure 7, where we see no evidence for degeneracies. The  $\Delta S^2$  between identical models is now  $\Delta S^2 = 0.258$ . The left plot indicates that mass parameters can shift by at most 20%. The right plot shows no evidence for bimodal behavior in the electroweak-ino sector.

We simulated  $m = 27196$  models, and still found a number of identical doubles,  $N_2 = 56$ . This gives us an estimate for the total number of bins in signature space

$$N_{sig} \sim m^2/N_2 \sim 6.6 \times 10^6 \quad (16)$$

which is somewhat larger than in our previous example, despite the smaller range of parameter space scanned. This clearly indicates that new leptonic directions in signature space are being opened up and we should expect fewer degeneracies.

Indeed, of the 56 degeneracies we found, *none* correspond to reasonably “different” models, which by equation (3) yields

$$\langle d \rangle \sim 1. \quad (17)$$

The pigeonhole principle argument also gives us an estimate of the number of degeneracies in the cascade decay with on-shell sleptons. Suppose we could have the following accuracies on the measurement of soft parameters: gluinos to 50 GeV, both left- and right-handed squarks to 75 GeV, both left- and right-handed sleptons to 75 GeV, and electroweak-inos to 50 GeV. This gives us<sup>6</sup>

$$N_{models} \sim 2 \times 4^3 \times 6^2 \times 10^3 \sim 5 \times 10^6 \sim N_{sig}, \quad (18)$$

So by equation (5), we should be left with some  $\mathcal{O}(1)$  number degeneracies in this case.

The reduction of the number of the degeneracies in this scenario can also be seen in the  $(\Delta S^2, \Delta P^2)$  plots shown in figure 25. More quantitatively, the number of expected

<sup>6</sup>Again, these values are chosen by estimating the local variation in mass parameters from  $(\Delta S^2, \Delta P^2)$  plots for our cascade run. However, the separate plots for gluinos, squarks, sleptons, and electroweak-inos are not shown in this paper.

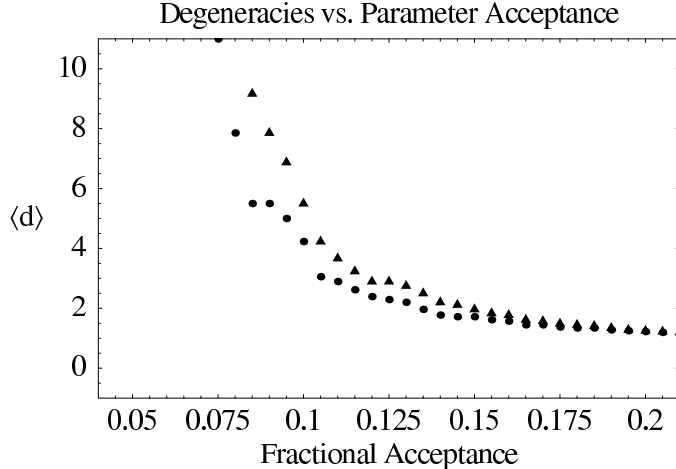


Figure 26: Number of degeneracies as a function of allowed fractional error in cascades run. Triangles correspond to imposing the fractional acceptance on gaugino, higgsino, and squark parameters. Dots correspond to just imposing fractional acceptance on the inos. We see that the number of degeneracies asymptotes to 1, indicating that the only “degeneracies” we have observed are coming from uncertainties in mass measurements and not from discrete choices in the spectrum.

degeneracies as a function of fractional differences in the parameters is shown in figure 26. As we discuss more below, the reduction in the number of degeneracies is mainly due to the fact that with long decay chains, it is in general much harder to find flippers in the electroweak-ino sector. Notice also that the number of degeneracies including squarks in figure 26 is also much smaller compared with our general scan. This is partly due to the fact that we have chosen the three generations of soft masses to be universal, but equally important, our better handle on the identities of the electroweak-inos from sleptons translates into a better handle on the left-right splitting of the squarks.

The main reason that the presence of the sleptons significantly reduces the number of degeneracies is their role in decays of the type shown in figure 27. Without sleptons in the decay chain, the electroweak-ino decays are typically dominated by  $W/Z$ s—the left panel of figure 27—and Higgses. Because  $h \rightarrow b\bar{b}$  typically carries less information due to backgrounds and tagging efficiencies, the only robust handle on electroweak-ino decays comes from leptonically decaying  $W$ s and  $Z$ s. However, this handle is of limited value, because we not only lose statistics because of the small leptonic branching ratio of  $W/Z$ , but we also lose information about the electroweak-ino identity because the leptons are not directly coupled to them.

On the other hand, the situation is significantly better with (on-shell) sleptons in the

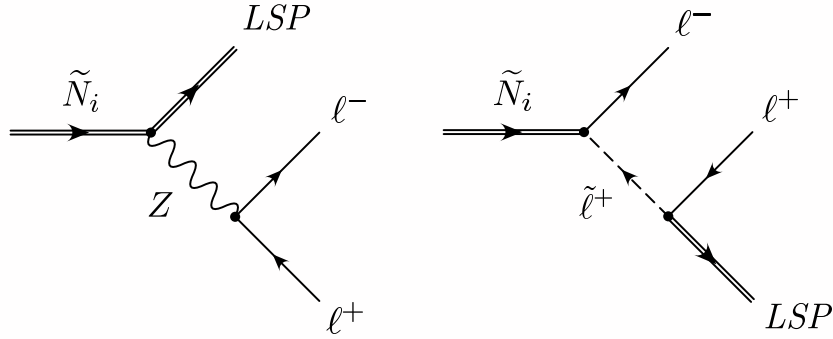


Figure 27: The two major processes that can lead to correlated same-flavor opposite-sign dileptons in SUSY cascade decays. When dileptons come mostly from on-shell  $Z$  bosons as in the left diagram, then crucial information about the masses and identities of the neutralinos is lost. Only when sleptons are copiously produced in cascade decays as in the right diagram, do we gain a strong handle on the identities and mass splittings of neutralino spectrum.

decay chain. The leptonic branching ratios as well as the charge of the leptons are sensitive to the identities of the electroweak-ino states in decay processes of the type shown in the right panel of figure 27. In addition, slepton edges [33, 34, 35, 37] give a strong constraint on the mass difference between electroweak-inos, further limiting the possibilities for degeneracies.

Still, we expect that in some cases it should be possible to flip the identities of the electroweak-inos in combination with flips of the other sfermion states. One example of such a flipper is shown in figure 28, though strictly speaking this pair of models does not satisfy the degeneracy criteria of section 4.3. In this example, the left- and right-handed squark states flip in order to accommodate a flip of the bino and wino. On the other hand, this is not a perfect example, since the sleptons are still somewhat decoupled except through small mixings between the higgsinos and the gauginos.

If there do exist left-right flippers involving sleptons, we expect them to be subtle since they have to reproduce a large amount information contained in the leptonic signatures. In the case that non-degenerate left- and right-handed sleptons are produced in cascade decays, it would be extremely difficult to flip the wino and bino around the slepton states; a scenario with heavier bino will have two edges in the dilepton invariant mass spectrum, while a scenario with a heavier wino will only have one edge.

On the other hand, there could be other scenarios in which we could have a flipper. Two of those possibilities are shown in figure 29. It is possible that sleptons in the decay chain have near universal masses, as shown in the left panel. It is also possible the left- and right-handed sleptons are playing different roles in the bino-wino flip case, as shown in the right

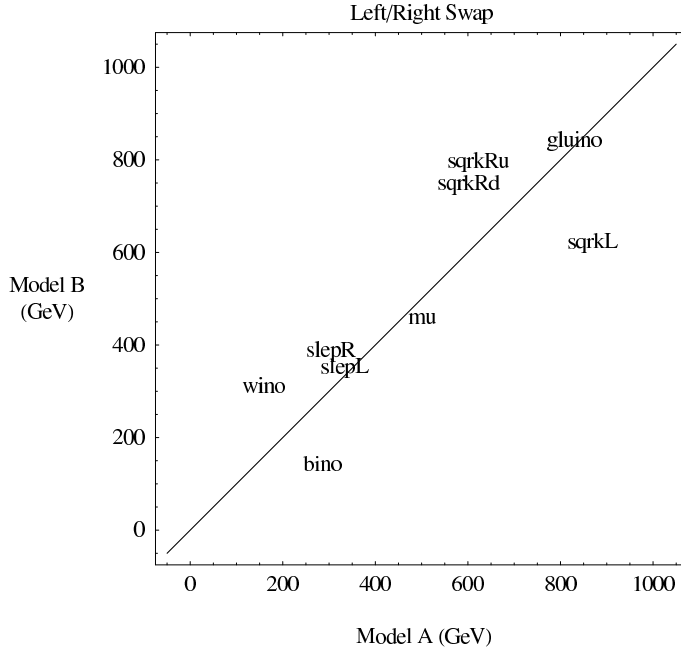


Figure 28: An example of a Left/Right Flipper. Though this example does not fall within the  $(\Delta S)^2$  cut that defines typical statistical fluctuations, the models are sufficiently close in signature space that slight adjustments in the colored sector might make this a real degeneracy. In this example, the left- and right-handed sfermions switch places to accommodate a bino-wino flip.

### Cascade Left/Right Swap?

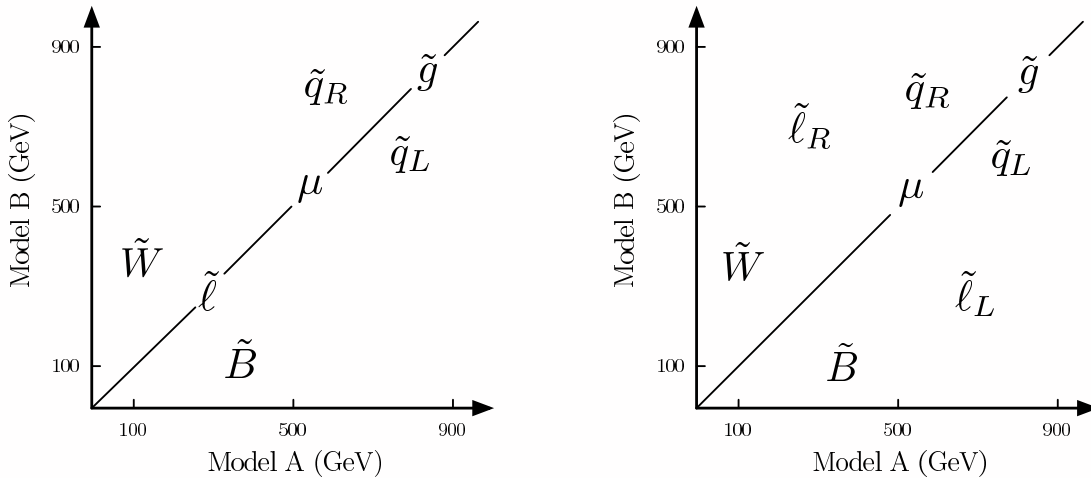


Figure 29: Possible examples of Left/Right Flippers involving copious slepton production. In order to avoid a double slepton edge from bino decays, either the sleptons must be nearly degenerate, or only one handedness of slepton can be involved in the decay.

panel. In both of these cases, a double edge [43, 44] would not exist, but it may be the case that these models could be distinguished by a subtle difference between dilepton and trilepton events. Verifying the existence of such degeneracies is a challenging task.

## 8 Future Directions

As mentioned in section 4, we have made two main compromises in our study of the inverse map by not including standard model background and by only simulating  $10 \text{ fb}^{-1}$  of data. In order to fully realistically assess the potential of measuring SUSY parameters at LHC, these two issues must be addressed.

Various significant components of standard model backgrounds to SUSY signatures—such as di-boson,  $t\bar{t}$ , and  $W/Z + \text{jets}$ —have been studied for supersymmetry searches [27, 28]. The presence of standard model background will no doubt worsen the sensitivity of LHC observables, in particular pure jet signals, to soft parameters. Therefore, it is crucial to study the extent to which it will change the number or structure of the degeneracies.

Similarly, the LHC is going to achieve a much larger luminosity than we have simulated. With a higher luminosity of  $\sim 300 \text{ fb}^{-1}$ , we could in principle introduce more stringent cuts to purify the signal without losing statistical significance. Therefore, compared with our study, a full LHC data set with high luminosity will significantly reduce statistical fluctuations, and a fully realistic characterization of the inverse map will have to take this into account as well. In addition, a number of processes that can only be observed with larger rates might be valuable in removing degeneracies.

The list of observables in appendix B are by no means exhaustive, nor are the selection cuts completely optimized. Our study shows that in order to break degeneracies at the LHC it is very important to construct new independent observables, and it may be possible to optimize the event selection criteria, or use multiple selection criteria, to increase the effective dimensionality of signature space. Furthermore, observables such as  $g_\mu - 2$ , dark matter detection and density, and perhaps  $B_S \rightarrow \mu^+ \mu^-$  depend on on the same parameters in different ways, and might be important in removing degeneracies. They could simply be added as additional signatures for each model.

One of the major reasons for the existence of degeneracies is the loss of information due to the hadronization and the formation of jets. One possible direction that deserves much more careful study is how much, information about the initial parton we can get out of a jet in addition to its four-momentum, by including the information such as track charge

weighted by energy [45], or better observables for the same physics. A measurement of jet charge with any significant confidence would be very effective in removing degeneracies if it were possible. On the other hand, due to the large statistics of the jet signatures, even some small preference at the percentage level could help in principle.

Supersymmetry events usually have a large number of jets from different decay chains, as well as from different parts of the same decay chains. Therefore, even with a pure signal sample, important structures in the jet kinematical distributions are usually swamped by combinatorial backgrounds. It will be necessary to develop more sophisticated methods of pairing up the correct combinations of jets if we are to extract useful information about decay kinematics.

Because leptonic signatures are so informative, it would be helpful if we could get as many leptonic events as possible. It is possible to enhance the leptonic signature by using smarter cuts in special cases. For example, in certain scenarios, leptons could tend to be very hard while the jets are softer. In this case, a better selection criteria would focus on events with hard leptons instead of imposing such strong cuts on the jets. Careful study of using different cuts for each of two or more leptons could be useful.

Since we expect the sizes of degenerate islands to be small, and because the dimensionality of the parameter space is large, it is very difficult to scan densely and simulate a sizable sample of data at each step. One possible method for identifying degeneracies is to carry out a leading order scan by matching a limited set of important  $\text{rate} \times \text{branching}$  ratios to narrow down potential regions. Such a scan will not require event simulation and hence is much less time/resource consuming. After such an initial scan, we could then start to scan and simulate in a much narrower region in order to search for and identify degeneracies.

A particularly interesting example of a degeneracy study would be based on the mSUGRA model SPS1a [46]. This model has an on-shell slepton in the decay chain and hence strong multi-lepton signals. Based on our study, we should have less freedom in such a scenario to move the soft parameters around—especially the slepton and electroweak-ino masses—without producing large difference in observables. On the other hand, even in this case, we still expect to see more delicate flippers which combine the flipping of the bino and wino with shifts in the sfermion masses. Therefore, it would be interesting to do a dedicated study to find generic SUSY models degenerate with SPS1a. The most important outcome of such a study would probably be a systematic method for mapping out degeneracies.

Another way to understand degeneracies is to try to determine the shapes of the small islands in parameter space. Though we found in our study that the size of regions in the

parameter space corresponding to a signature bin were small, if we had more details about the shape of the small islands in each direction of parameter space, it would help us in mapping out the set of solutions matching LHC data. One such study could be based on parameter excursions around a generic set of MSSM models and one could measure the rate that signatures change in different parameter directions.

Measuring the difference between left-handed and right-handed squarks turns out to be quite difficult. We expect the overall rate will fix roughly some overall scale of the squarks. Although the structure in left-right squark degeneracies is much less prominent than the case of electroweak-inos, such a splitting is not expected to be a flat direction either. Therefore, details of a left-right squark degeneracy remain one of the important directions that need further exploration.

Of course, the statistical method we have developed in this study is completely general and applicable to any class of models. It is important to repeat the same analysis not only within a class of models for new physics but also between such classes. In particular, it will be interesting to observe the inverse maps of models with similar gauge quantum numbers to SUSY, such as universal extra dimensions or the little Higgs with  $T$ -parity. Understanding robust distinctions between those models and supersymmetry is one of the most important questions in interpreting LHC data.

## 9 After a Discovery at the LHC

If new physics is discovered at the LHC with a pattern of signals roughly consistent with SUSY, the most pressing challenge will be to invert the LHC signatures and extract information about the soft supersymmetry breaking parameters.

An obvious first step is finding *any* model that fits the set of LHC signatures that have been measured, presumably starting with a reduced set of SUSY parameters. Our study shows that the success in finding one model which fits the data is not the end of the process, though. In generic regions of SUSY parameter space, if there are not significant additions to the list of signatures we have used, there will be different models which produce indistinguishable signatures. The number of degeneracies is not intractably large, suggesting that degenerate models may be distinguishable with more detailed study.

Therefore, the most important task after finding one model that fits the LHC data is to create a catalog of all models which have signatures consistent with observation. The reason is that any detailed study would presumably require the construction of special observables

designed to distinguish specific models. Due to the small size of the islands in the parameter space occupied by degenerate models, and the large volume in which those islands are scattered, mapping out degeneracies is challenging. The naive approach of carpeting parameter space will not work in this case because of the large amount of necessary computation.

Clearly, new methods and insights need to be developed for the purpose of identifying potential degeneracies. However, our characterization of the possible degeneracies as flippers, sliders, and squeezers is a useful first step in finding other candidate models. Then again, even though there are simple characterizations of the degeneracies in the electroweak-ino sector, we saw that other soft parameter had to shift to accommodate such changes, complicating the task of manufacturing degeneracies. There have been some attempts to match parameters of supersymmetry breaking with LHC data [37, 38, 39, 47], and it would be interesting to see whether these approaches can be modified for the purpose of finding degeneracies.

## 10 Discussion and Outlook

In two years, the LHC will begin to answer questions that have driven much of the theoretical activity in our field for the past three decades. Thinking about how we will go from LHC data to the underlying model *now* will help us get to the physics we really care about as quickly as possible, and may be able to improve experimental settings and procedure. In this paper, we have initiated a systematic study of the LHC inverse problem, within the context of the supersymmetric standard model with minimal particle content but (relatively) unconstrained parameter space. We have used simple statistical techniques to probe this map, in particular studying the average number of models with equivalent LHC signals, and the effective dimensionality of the signature space populated by SUSY.

In the regions of parameter space where the sleptons are not produced in long cascade decay chains, we find that there is very little handle on the slepton masses, and degeneracies in the electroweak-ino sector. The typical number of degeneracies for any given model is of order  $\langle d \rangle \sim 10 - 100$ . We have shown that these degeneracies have simple interpretations. For instance, in the decay of  $\chi_2^0$  to  $\chi_1^0$ , we can have “flippers” where  $(\chi_2^0, \chi_1^0)$  are either  $(\tilde{B}, \tilde{W})$  or  $(\tilde{W}, \tilde{B})$ , with accompanying changes in the rest of the spectrum to match LHC signatures. With sleptons produced on-shell in cascade decays as is the case in many of the well-studied mSUGRA models, but perhaps not in nature, the situation is better, but there may still be possible degeneracies involving left/right swaps.

Our study of the inverse problem reconciles two orthogonal views one often hears about

what the LHC can determine about weak-scale physics. There is the school of thought that says that the LHC is only a discovery machine, but that any more precise determination of the underlying physics must await the construction of a linear collider. Another school of thought holds that not only can the LHC discover new physics, it can also determine model parameters to few percent accuracy! Our picture of the inverse map shows the sense in which both of these pictures can be correct. There can indeed be a relatively large number of different models compatible with LHC data, partially justifying the first view, but each of these is a small island in parameter space, partially justifying the second view. Our result for the number of degeneracies  $\sim 1 - 100$  is as interesting as it could have been, however. The number is not  $10^6$ ; it is just large enough to represent a non-trivial challenge and just small enough to spur us to think of clever new signatures to resolve the small number of ambiguities in SUSY. And it is easy to determine whether a new set of signatures is effective in enlarging signature space—we simply add the signature and compute the new average number of degeneracies  $\langle d \rangle$ .

Obviously, the number of degeneracies will be smaller if a more restrictive parameter space is chosen. Again, this can be looked at by repeating our analysis for the restricted models and computing  $\langle d \rangle$ . If  $\langle d \rangle \sim 1$ , then if such a simple model reproduces LHC data, it is not likely to have a degenerate pair within its own model space, and despite the fact that it may have  $\sim 1 - 100$  degenerate pairs in an enlarged parameter space, it would clearly be preferred over other generic points. It is quite interesting that  $\tan\beta$  is difficult to measure in general, and it is challenging to find signatures that are sensitive to  $\tan\beta$  alone. Perhaps when information about the superpartner spectrum is known from the LHC,  $\tan\beta$  could be determined with other information that is very sensitive to  $\tan\beta$ , such as the higgs sector,  $g_\mu - 2$  and  $B_S \rightarrow \mu^+\mu^-$  constraints.

We have illustrated our approach to the inverse problem in the context of low-energy SUSY, but the same ideas can be applied to any theory of physics beyond the standard model, including theories of extra dimensions with KK parity and of little Higgs models with T-parity, which have very similar signatures to SUSY. Indeed, SUSY is likely a more challenging example due to its large parameter space. It would be interesting to study the inverse map in other models and between other models, study how the model footprints differ in signature space, and test ways of distinguishing qualitatively different possibilities for new physics at the LHC. Furthermore, our entire discussion has been at the electroweak scale in four dimensions. Once the 4D effective lagrangian is determined at the weak scale, we can begin probing the underlying higher scale or higher dimensional physics.

**Acknowledgments:** We are deeply indebted to Michael Busha, Suvendra Dutta, Gus

Evrard, and Matias Zaldarriaga for valuable computing time and computing expertise at two cluster machines: “Sauron” at the Harvard Center for Astrophysics and “Opus” at the Computing for the Natural Sciences Group, University of Michigan. We thank Kevin Black, Matt Bowen, Michael Douglas, Can Kilic, Fabiola Gianotti, Tao Han, John Huth, Amit Lath, Rakhi Mahbubani, Shawn McKee, Brent Nelson, Michael Peskin, Aaron Pierce, Albert de Roeck, Maria Spiropulu, Scott Thomas, Chris Tully, Devin Walker, and James Wells for interesting discussions. We especially thank Matt Strassler and Steve Mrenna for valuable insights into detector simulations and for helping us incorporate PGS in this study. The work of NAH, JKT, and LTW is supported by the DOE under contract DE-FG02-91ER40654. The work of GLK is supported in part by the DOE. LTW and GLK thank the Aspen Center for Theoretical Physics for hospitality while part of this work was carried out. LTW also thanks the support and hospitality of the Michigan Center for Theoretical Physics during several stages of this work.

## A N-tuples and Demonic Bins

In section 2.3 we derived a value for  $N$ , the number of experimentally distinguishable outcomes at the LHC, making the assumption that each signature bin is equally likely to be occupied. We can improve on this very simple picture. For instance, it could be that some fraction of bins are “demonic”, in the sense that a disproportionate number of balls land into them. We can model this by saying that a fraction  $x$  of balls land into a fraction  $\lambda$  of the bins, while the remaining fraction  $(1 - x)$  of the balls land into the  $(1 - \lambda)$  fraction of bins. The number of expected  $p$ -tuples of balls in the same bin is then

$$N_p \sim \frac{m^p}{p!N^{p-1}} \left( \frac{x^p}{\lambda^{p-1}} + \frac{(1-x)^p}{(1-\lambda)^{p-1}} \right). \quad (19)$$

We can fit the observed  $N_p$  to determine  $N, x, \lambda$ .

In our sample of with  $m = 43026$ , we have 283 doubles, 32 triples, and 3 quadruples, which is consistent with

$$N = 3.19 \times 10^7, \quad x = 0.0317, \quad \lambda = 0.000114, \quad (20)$$

telling us that 3.2% of models map to 0.01% of signature space. However, with such low statistics it is difficult to say whether this picture is correct, because we are fitting three numbers with three parameters. To really check the picture, we can artificially increase the statistics by going to a larger signature cut to define degenerate models. If we increase the

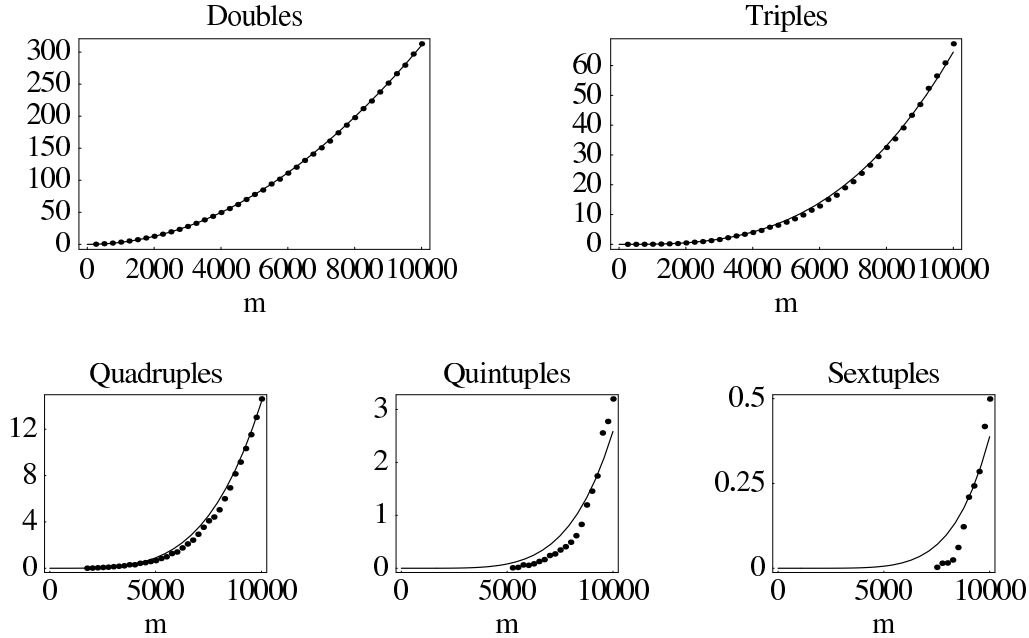


Figure 30: The fits of  $N_p$  to equation (19). The  $m$  axis indicates the number of models simulated, and in order to make smooth curves, 1000 random choices for the  $m$  models were averaged for each data point. The number of  $p$ -tuples is consistent with the picture that 4.7% of models map to 0.11% of signature space, indicating that while 5% of models are much more likely to have degeneracies than generic models, the phenomena of degeneracies is not completely dominated by small regions in parameter space.

number of doubles by a factor of 20, this gives us a sizable number of  $p$ -tuples, and we can now fit the  $N_p$  curves as a function of  $m$ . Because we have 43,026 models to work with, we can average over many different subsets containing  $m$  models to get a smooth curve for  $N_p$  as a function of  $m$ .

The curves shown in figure 30 are for

$$N = 4.65 \times 10^5, \quad x = 0.0473, \quad \lambda = 0.00113, \quad (21)$$

which tells us that 4.7% of the models map to 0.11% of the signature space. Because we have artificially increased the number of doubles by a factor of 20, the real value of  $N$  should be 20 times bigger than the value in equation (21), giving us

$$N = 9.3 \times 10^6, \quad (22)$$

which is roughly compatible with equation (20).

## B Complete List of LHC Observables

In this section, we summarize the LHC signatures we have included in our study. The signatures can be divided into two categories: counting signatures and kinematical distributions. Both types of signatures depend crucially on the cuts and triggers we impose to isolate a signal sample.

### B.1 Cuts and Triggers

We identify our signal sample through a set of event filtering triggers and selection cuts. To account for the effect of multiple interactions and initial state radiation (which yield additional soft objects in events), we only keep objects in the event record if

$$\text{photon, leptons: } P_T > 20, \quad |\eta| < 2, \quad \text{jets: } P_T > 50, \quad |\eta| < 3. \quad (23)$$

We then select events with two or more jets subject to the criteria that

$$\cancel{E}_T > 150 \text{ GeV}, \quad H_T > \begin{cases} 600 \text{ GeV} & \text{0 or 1 lepton in event} \\ 400 \text{ GeV} & \text{2 or more leptons in event} \end{cases}, \quad (24)$$

where

$$H_T = \cancel{E}_T + \sum_{\text{all jets}} P_T^a. \quad (25)$$

These cuts were not optimized to maximally enhance signal over standard model background. However, the number of standard model events that pass these cuts are reasonable—a  $10 \text{ fb}^{-1} t\bar{t}$  sample contains around 76000 events that satisfy the above criteria out of  $4.9 \times 10^6$  events total.

### B.2 Counting Signatures

Counting signatures record the number of a specific kind of events based solely on their object content. The most inclusive counting signature is the total number of events that passes the trigger and cuts. All other counting signatures are represented as ratios to the total number of events or as ratios to each other.

The only distinction between jets is whether they are  $b$ -tagged.<sup>7</sup> Therefore, we count jet multiplicity in two categories,  $b$ -jet and non- $b$ -jet. On the other hand, the leptons carry both charge and flavor information, so we keep separate counts for each charge and flavor

---

<sup>7</sup>Strictly speaking, the  $b$ -tag algorithm in PGS is a heavy-flavor tag and thus includes some  $c$ -quark jets.

configuration. Supersymmetric events could have multiple photons associated with them both from initial and final state radiation, as well as decay products. Therefore, a typical classification of a counting signature could be represented as

$$\text{jets}(\#\text{non-}b\text{-jet}, \#\text{b-jet}) + \text{leptons}(\#, \text{charge}, \text{flavor}) + \#\gamma + \cancel{E}_T. \quad (26)$$

Of course, we could form more inclusive observables by combining several categories together. For example, we could have an inclusive signature for the number of events with 1 lepton (including all possible charges and flavors) and 2 non- $b$ -jets.

Now, we list the counting signatures that we have implemented. Where appropriate, we use the following shorthand to define ratios.

$$\frac{Y}{X} \rightarrow \frac{\text{Number of events with X and Y}}{\text{Number of events with X}} \quad (27)$$

1. Total number of events.

The sum of all events that passed the selection cuts.

2. Jet and lepton counts.

Events are categorized according to the number of leptonic objects in the event. All counts here are charge and flavor inclusive. For each lepton number category, the counts are further separated according to number of jets and  $b$ -jets in the event. The signatures are:

$$\frac{n_\ell \text{ leptons}}{\text{total events}}, \quad \frac{n_j \text{ jets}}{n_\ell \text{ leptons}}, \quad \frac{n_b \text{ b-jets}}{n_\ell \text{ leptons}}, \quad (28)$$

where

$$n_\ell = 0, 1, 2, 3, 4^+, \quad n_j = 2, 3, 4, 5, 6, 7, 8^+, \quad n_b = 0, 1, 2, 3, 4, 5, 6^+. \quad (29)$$

Note that  $n_j$  jets includes both  $b$ -jets and non- $b$ -jets.

3. Lepton flavor and charge counts.

For events with leptons, flavor information is used to further divide signatures into sub-categories. We have included here only the overall counting of the different flavor/charge categories without regard for jet multiplicity. In all cases, the signature used is

$$\frac{\text{flavor category}}{n_\ell \text{ leptons}}, \quad (30)$$

where the flavor categories are:

- 1 $\ell$ . 6 possibilities  $\ell_i^\pm$  ( $i = e, \mu, \tau$ ).
- 2 $\ell$ . 21 combinations  $\ell_i^\pm \ell_j^\pm$ .
- 3 $\ell$ . For events with 2 same flavor opposite charge leptons  $\ell_i^+ \ell_i^- \ell_j^\pm$ , we categorize them according to the flavor of  $\ell_i$  and the flavor/charge of  $\ell_j^\pm$ . (18 combinations.) For trilepton events without same flavor opposite charge pairs, we give the total charge ( $1\pm, 3\pm$ ) and the dominant flavor ( $e, \mu, \tau$ ). (12 combinations.) When the dominant flavor is ambiguous, we assign the dominant flavor to be  $\tau$ .
- 4 $^+\ell$ . We do not include flavor/charge information in this category.

4. Photon counts.

$$\frac{n_\gamma \text{ photons}}{\text{total events}}, \quad n_\gamma = 0, 1, 2^+. \quad (31)$$

### B.3 Kinematical Distributions

Generally, separate distributions for certain kinematic variables can be implemented according to the object content of the event, as in equation (26). For a lot of inclusive distributions we have used in this analysis, we use the number of leptons, jets, and  $b$ -jets to label the distribution.

The kinematical distributions are divided into two broad categories:  $P_T$  (those based on transverse momentum sums) and  $m_{\text{inv}}$  (those based on Lorentz-invariant four-vector sums).

#### B.3.1 Transverse Momenta: $P_T$

In this category, all kinematical observables has the form

$$\sum_{\{a\}} P_T^a, \quad (32)$$

where the sum is over a set of specific objects of interest. Distributions are always binned into deciles, and the boundaries of the deciles (excluding the overall lower and upper bounds) are the signatures we store.

The most commonly used observable in this category is effective mass,  $M_{\text{eff}}$  [27, 28, 31, 33]. Instead of defining  $M_{\text{eff}}$  only for the jet signatures, we define such an observable for any large class of event objects,

$$M_{\text{eff}} = \cancel{E}_T + \sum_{\text{all objects}} P_T, \quad (33)$$

Notice that instead of summing the  $P_T$  of just the jets, we sum the  $P_T$  for all objects in the events. We separate  $M_{\text{eff}}$  into 12 different distributions labeled by the number of jets and leptons in the event:

$$n_j = 2, 3, 4, 5^+, \quad n_\ell = 0, 1, 2^+. \quad (34)$$

In particular,  $M_{\text{eff}}(n_j, n_\ell)$  only includes events with exactly  $n_j$  jets and  $n_\ell$  leptons.

We have also implemented inclusive distributions of jets, leptons, photons, and  $\cancel{E}_T$ .

- $P_T^{nhj}$ . Inclusive  $P_T$  distribution of the  $n$ -th hardest jet, where  $n = 1, 2, 3, 4$ . Distributions are categorized according to number of leptons ( $n_\ell = 0, 1, 2^+$ ) but include all events with at least  $n$  jets.
- $P_T^\ell$  for all events with leptons. Separate distributions are used for different lepton flavor, but there is no charge separation, nor separation by the number of jets in the event.
- $P_T^\gamma$  for all events with photons.
- $\cancel{E}_T$  for all events that pass our trigger. Separate distributions are used for different number of leptons ( $n_\ell = 0, 1, 2^+$ ).

### B.3.2 Invariant Mass: $m_{\text{inv}}$

In this category, all kinematical observables have the form

$$\left( \sum_{\{a\}} p_\mu^a \right)^2. \quad (35)$$

Invariant mass distribution typically carry important information about the masses of the massive particles in the decay chain. They have been used extensively in the past in studies for measuring soft parameters [33, 34, 35, 37]. We have implemented in our study a collection of invariant mass distributions which, if well populated, are sensitive to all important masses of superpartners. Unless otherwise indicated, invariant mass distributions are binned into deciles.

1. All objects.

Invariant mass for all the objects in the event are used in there distributions. Separate distributions are created according to number of lepton and jets in the event:

$$n_j = 2, 3, 4, 5^+, \quad n_\ell = 0, 1, 2^+. \quad (36)$$

## 2. Jet objects.

Invariant masses of various combinations of jets are used, if such a combination is possible in the event. Events are further divided into separate distributions based on the number of leptons in the event ( $n_\ell = 0, 1, 2^+$ ). We use the following shorthand notation in events with many jets:  $h$  refers to the hardest jet regardless of flavor,  $n$  refers to the hardest non- $b$ -jet;  $b$  refers to the hardest jet with a  $b$ -tag. In all but the di- $b$ -jet invariant mass distribution, these distributions are inclusive of the total number of jets; for example, the invariant mass distribution for the two hardest jets includes all events with at least two hard jets.

- $m_{hh}$ . Two hardest jets.
- $m_{hhh}$ . Three hardest jets.
- $m_{hhhh}$ . Four hardest jets.
- $m_{nn}$ . Hardest pair of non- $b$ -jets.
- $m_{bn}$ . Hardest  $b$ -jet paired with hardest non- $b$ -jet.
- $m_{bnn}$ . Hardest  $b$ -jet with two hardest non- $b$ -jets.
- $m_{bb}$ . Pairs of  $b$ -jets in events with exactly 2  $b$ -jets, binned in 20-tiles.
- $m_{bbn}$ . Two hardest  $b$ -jets with hardest non- $b$ -jet.
- $m_{bbnn}$ . Two hardest  $b$ -jets with 2 hardest non- $b$ -jets.

## 3. Events with one lepton.

For events with a single lepton, we construct invariant mass distributions involving the hardest jets ( $h$ ) and hardest  $b$ -tagged jets ( $b$ ). All distributions are separated by lepton flavor but not by charge, and placed into 20-tiles.

- $m_{\ell,h^{1,2}}$ . Separate distributions for combining the single lepton with the first or second hardest jet.
- $m_{\ell,b^{1,2}}$ . Separate distributions for combining a single lepton with the first or second hardest  $b$ -jet.

## 4. Events with same-flavor opposite-sign dileptons.

For events with dileptons, we have included various invariant mass distributions, many of them similar to those studied in [34, 35]. The existence of dileptons indicates a long decay chain with at least two jets from earlier stage of the same decay chain. Various

pairing of the leptons and jets are sensitive to a variety of combinations of the masses of the superpartners involved—squarks, electroweak-inos, and possibly the sleptons.

All dilepton invariant mass distributions refer to events with same-flavor opposite-sign dileptons and no other leptons, with separate distributions for different dilepton flavors. All distributions are binned in 20-tiles excepted where noted.

- $m_{ll}$ . Dilepton invariant mass distribution. Dilepton pairs whose invariant mass falls in the range  $\pm 5$  GeV of  $m_Z$  are subtracted and histogrammed in a separate distribution. The ratio of the number of events in the “ $Z$ -window” to the total number of dileptons is used as an additional signature.
- $m_{\ell\ell,b}$ . Pair of leptons with the hardest  $b$ -jet in events with at least 1  $b$ -jet.
- $m_{\ell\ell,hh}$ . Pair of leptons with the two hardest jets.
- $m_{\ell\ell,h^{\text{high,low}}}$ . Combination of first or second hardest jet with the pair of leptons. High (low) are defined by the combination with the larger (smaller) invariant mass. The jet associated with the high (low) combination is labeled as high (low) for the distribution below.
- $m^{\text{high,low}}(\ell, h^{\text{high,low}})$ . Four combinations of combining the high or low jet with each lepton, choosing the lepton that gives rise to the larger ( $m^{\text{high}}$ ) or smaller ( $m^{\text{low}}$ ) invariant mass.

The following histogram are for events with exactly 2  $b$ -jets and dileptons. Because these histograms are generically less populated than the ones above, they are binned only in deciles.

- $m_{bb|\ell\ell}$   $bb$  invariant mass distribution in dilepton events.
- $m_{bb\ell\ell}$ . Pair of leptons with both  $bs$ .
- $m_{bb\ell}^{\text{high,low}}$ .  $b$ - $b$ -lepton invariant mass, where high (low) refers to the lepton that gives the largest (smallest) invariant mass.
- $m_{\ell\ell,b^{\text{high,low}}}$ . Combination of first or second hardest  $b$ -jet with the pair of leptons. High (low) are defined by the combination with larger (smaller) invariant mass. The jet associated with the high (low) combination are labeled as high (low) for the distribution below.
- $m^{\text{high,low}}(\ell, b^{\text{high,low}})$ . Four combinations of combining the high or low  $b$ -jet with each lepton, choosing the lepton that gives rise to the larger ( $m^{\text{high}}$ ) or smaller ( $m^{\text{low}}$ ) invariant mass

5.  $m_{\gamma\gamma}$ . Di-photon invariant mass distribution, in deciles.

## C Technique for Assigning Statistical Error Bars

To assign error bars to our signatures, we use Gaussian statistics supplemented with  $\mathcal{O}(1)$  scale factors. We ignore systematic errors and errors from standard model background subtraction. Using a detector simulator, the best way to determine statistical errors is to run a model many times at fixed integrated luminosity to figure out the appropriate confidence intervals on a given signature. This is very computationally expensive, so we will use a simple method to mock up reasonable error bars.

For every signature we first define a raw statistical error bar based on Gaussian statistics. For an integer-valued counting signature of value  $n$ ,

$$\delta_{\text{raw}}n = \sqrt{n+1}. \quad (37)$$

For a ratio-valued counting signature of value  $n/m$ , where  $n$  and  $m$  are pseudo-independent integer-valued counts,

$$\delta_{\text{raw}}\left(\frac{n}{m}\right) = \sqrt{\left(\frac{\sqrt{n+1}}{m+1}\right)^2 + \left(\frac{n\sqrt{m+1}}{(m+1)^2}\right)^2}. \quad (38)$$

For a histogram with  $n$  elements and a quantile boundary with value  $q$ , we define  $q_{\text{low}}$  ( $q_{\text{high}}$ ) as the new value of the quantile boundary if  $\sqrt{n}$  elements were added to the lowest (highest) bin of the histogram. The raw statistical error on  $q$  is defined as

$$\delta_{\text{raw}}q = \sqrt{\frac{(q - q_{\text{low}})^2 + (q - q_{\text{high}})^2}{2}}. \quad (39)$$

While these raw statistical error bars scale like Gaussian statistics, there is no guarantee that Gaussian statistics is a good description of the errors from PYTHIA piped through PGS. Therefore, for the  $i$ -th signature, we define the statistical fluctuation as

$$\delta_{\text{stat}}s_i = \alpha_i\delta_{\text{raw}}s_i, \quad (40)$$

where  $\alpha_i$  is an  $\mathcal{O}(1)$  phenomenological parameter that is different for each signature. To determine the value of  $\alpha$ , we ran a subset of our models again with a different random number seed. Then for every signature, we calculate

$$\alpha_i^{12} = \frac{|s_i^1 - s_i^2|}{\sqrt{(\delta_{\text{raw}}s_i^1)^2 + (\delta_{\text{raw}}s_i^2)^2}}, \quad (41)$$

where  $s_i^1$  and  $s_i^2$  are the signature values of the same model with different random number seeds. The  $\alpha_i$  we use in subsequent calculations is the 95th percentile of  $\alpha_i^{1,2}$  taken over all models or 1, whichever is largest. The selected  $\alpha_i$  values never exceeded 2.2, telling us that Gaussian statistics are a good approximation to statistical error bars over a wide range of models and signatures.

## References

- [1] S. Dimopoulos and H. Georgi, Nucl. Phys. B **193**, 150 (1981).
- [2] S. Weinberg, Phys. Rev. D **19**, 1277 (1979).  
L. Susskind, Phys. Rev. D **20**, 2619 (1979).
- [3] N. Arkani-Hamed, S. Dimopoulos and G. R. Dvali, Phys. Lett. B **429**, 263 (1998) [arXiv:hep-ph/9803315].  
N. Arkani-Hamed, S. Dimopoulos and G. R. Dvali, Phys. Rev. D **59**, 086004 (1999) [arXiv:hep-ph/9807344].  
I. Antoniadis, N. Arkani-Hamed, S. Dimopoulos and G. R. Dvali, Phys. Lett. B **436**, 257 (1998) [arXiv:hep-ph/9804398].
- [4] L. Randall and R. Sundrum, Phys. Rev. Lett. **83**, 3370 (1999) [arXiv:hep-ph/9905221].  
L. Randall and R. Sundrum, Phys. Rev. Lett. **83**, 4690 (1999) [arXiv:hep-th/9906064].
- [5] N. Arkani-Hamed, A. G. Cohen and H. Georgi, Phys. Lett. B **513**, 232 (2001) [arXiv:hep-ph/0105239].
- [6] C. Csaki, C. Grojean, L. Pilo and J. Terning, Phys. Rev. Lett. **92**, 101802 (2004) [arXiv:hep-ph/0308038].
- [7] K. Agashe, R. Contino and A. Pomarol, Nucl. Phys. B **719**, 165 (2005) [arXiv:hep-ph/0412089].
- [8] Z. Chacko, Y. Nomura and D. Tucker-Smith, Nucl. Phys. B **725**, 207 (2005) [arXiv:hep-ph/0504095].
- [9] K. Agashe, A. Delgado, M. J. May and R. Sundrum, JHEP **0308**, 050 (2003) [arXiv:hep-ph/0308036].
- [10] Z. Chacko, H. S. Goh and R. Harnik, arXiv:hep-ph/0506256.
- [11] T. Roy and M. Schmaltz, arXiv:hep-ph/0509357.  
C. Csaki, G. Marandella, Y. Shirman and A. Strumia, arXiv:hep-ph/0510294.
- [12] N. Arkani-Hamed, S. Dimopoulos, G. F. Giudice and A. Romanino, Nucl. Phys. B **709**, 3 (2005) [arXiv:hep-ph/0409232].  
N. Arkani-Hamed and S. Dimopoulos, JHEP **0506**, 073 (2005) [arXiv:hep-th/0405159].  
G. F. Giudice and A. Romanino, Nucl. Phys. B **699**, 65 (2004) [Erratum-ibid. B **706**, 65 (2005)] [arXiv:hep-ph/0406088].

- [13] N. Arkani-Hamed, S. Dimopoulos and S. Kachru, arXiv:hep-th/0501082.
- [14] P. C. Schuster and N. Toro, Phys. Rev. D **72**, 093005 (2005) [arXiv:hep-ph/0506079]. L. Senatore, arXiv:hep-ph/0507257. R. Mahbubani and L. Senatore, arXiv:hep-ph/0510064.
- [15] T. Appelquist, H. C. Cheng and B. A. Dobrescu, Phys. Rev. D **64**, 035002 (2001) [arXiv:hep-ph/0012100].
- [16] H. C. Cheng and I. Low, JHEP **0309**, 051 (2003) [arXiv:hep-ph/0308199].
- [17] H. C. Cheng, K. T. Matchev and M. Schmaltz, Phys. Rev. D **66**, 056006 (2002) [arXiv:hep-ph/0205314].
- [18] A. J. Barr, Phys. Lett. B **596**, 205 (2004) [arXiv:hep-ph/0405052].
- [19] T. Goto, arXiv:hep-ph/0411360.
- [20] J. M. Smillie and B. R. Webber, JHEP **0510**, 069 (2005) [arXiv:hep-ph/0507170].
- [21] H. C. Cheng, I. Low and L. T. Wang, arXiv:hep-ph/0510225.
- [22] A. Datta, G. L. Kane and M. Toharia, arXiv:hep-ph/0510204.
- [23] A. Datta, K. Kong and K. T. Matchev, arXiv:hep-ph/0509246.
- [24] A. J. Barr, arXiv:hep-ph/0511115.
- [25] P. Binetruy, G. L. Kane, B. D. Nelson, L. T. Wang and T. T. Wang, Phys. Rev. D **70**, 095006 (2004) [arXiv:hep-ph/0312248].
- [26] G. Kane, arXiv:hep-ph/0504257.
- [27] H. Baer, C. h. Chen, F. Paige and X. Tata, Phys. Rev. D **52**, 2746 (1995) [arXiv:hep-ph/9503271].
- [28] H. Baer, C. h. Chen, F. Paige and X. Tata, Phys. Rev. D **53**, 6241 (1996) [arXiv:hep-ph/9512383].
- [29] S. Mrenna, G. L. Kane, G. D. Kribs and J. D. Wells, Phys. Rev. D **53**, 1168 (1996) [arXiv:hep-ph/9505245].
- [30] S. Dimopoulos, S. D. Thomas and J. D. Wells, Nucl. Phys. B **488**, 39 (1997) [arXiv:hep-ph/9609434].
- [31] I. Hinchliffe, F. E. Paige, M. D. Shapiro, J. Soderqvist and W. Yao, Phys. Rev. D **55**, 5520 (1997) [arXiv:hep-ph/9610544].
- [32] T. Gherghetta, G. F. Giudice and J. D. Wells, Nucl. Phys. B **559**, 27 (1999) [arXiv:hep-ph/9904378].
- [33] For a summary of earlier studies, ATLAS Detector and Physics Performance Technical Design Report, Chapter 20  
<http://atlas.web.cern.ch/Atlas/GROUPS/PHYSICS/TDR/access.html>
- [34] B. K. Gjelsten, D. J. Miller and P. Osland, JHEP **0412**, 003 (2004) [arXiv:hep-ph/0410303].

- [35] B. K. Gjelsten, D. J. Miller and P. Osland, *JHEP* **0506**, 015 (2005) [arXiv:hep-ph/0501033].
- [36] B. K. Gjelsten, D. J. Miller and P. Osland, arXiv:hep-ph/0511008.
- [37] C. G. Lester, M. A. Parker and M. J. White, arXiv:hep-ph/0508143.
- [38] R. Lafaye, T. Plehn and D. Zerwas, arXiv:hep-ph/0404282.
- [39] P. Bechtle, K. Desch and P. Wienemann, arXiv:hep-ph/0511137.
- [40] G. Weiglein *et al.* [LHC/LC Study Group], arXiv:hep-ph/0410364.
- [41] T. Sjostrand, P. Eden, C. Friberg, L. Lonnblad, G. Miu, S. Mrenna and E. Norrbin, *Comput. Phys. Commun.* **135**, 238 (2001) [arXiv:hep-ph/0010017].  
<http://www.thep.lu.se/~torbjorn/Pythia.html>
- [42] PGS, Simple simulation package for generic collider detectors  
<http://www.physics.ucdavis.edu/~conway/research/software/pgs/pgs.html>
- [43] I. Hinchliffe and F. E. Paige, *Phys. Rev. D* **60**, 095002 (1999) [arXiv:hep-ph/9812233].
- [44] F. E. Paige and J. D. Wells, arXiv:hep-ph/0001249.
- [45] K. Abe *et al.* [SLD Collaboration], *Phys. Rev. Lett.* **74**, 2890 (1995).  
D. Buskulic *et al.* [ALEPH Collaboration], *Z. Phys. C* **71**, 357 (1996).  
P. Abreu *et al.* [DELPHI Collaboration], *Z. Phys. C* **72**, 17 (1996).  
R. Akers *et al.* [OPAL Collaboration], *Phys. Lett. B* **327**, 411 (1994).  
F. Abe *et al.* [CDF Collaboration], *Phys. Rev. D* **60**, 072003 (1999) [arXiv:hep-ex/9903011].  
X. Zhang, UMI-31-34389.  
P. Eerola [ATLAS Collaboration], *Nucl. Instrum. Meth. A* **384**, 93 (1996) [arXiv:hep-ex/9610002].
- [46] B. C. Allanach *et al.*, in *Proc. of the APS/DPF/DPB Summer Study on the Future of Particle Physics (Snowmass 2001)* ed. N. Graf, *Eur. Phys. J. C* **25**, 113 (2002) [eConf **C010630**, P125 (2001)] [arXiv:hep-ph/0202233].
- [47] B. C. Allanach, D. Grellscheid and F. Quevedo, *JHEP* **0407**, 069 (2004) [arXiv:hep-ph/0406277].